MATHEMATICAL MODELING OF SULFUR RETENTION IN FLUIDIZED BED COMBUSTORS

A THESIS SUBMITTED TO
THE GRADUATE SCHOOL OF NATURAL AND APPLIED SCIENCES
OF
THE MIDDLE EAST TECHNICAL UNIVERSITY

BY

HAKAN ALTINDAĞ

IN PARTIAL FULFILLMENT OF THE REQUIREMENTS FOR THE DEGREE OF

MASTER OF SCIENCE

IN

THE DEPARTMENT OF CHEMICAL ENGINEERING

AUGUST 2003

Approval of the Graduate School of Natural and Applied Sciences.

Prof. Dr. Canan Özgen
Director

I certify that this thesis satisfies all the requirements as a thesis for the degree of Master of Science.

Prof. Dr. Timur Doğu
Head of Department

This is to certify that we have read this thesis and that in our opinion it is fully adequate, in scope and quality, as a thesis and for the degree of Master of Science.

Dr. Olcay Oymak
Co-Supervisor

Prof. Dr. Nevin Selçuk
Supervisor

Examining Committee Members

Prof. Dr. İnci Eroğlu

Prof. Dr. Faruk Arınç

Prof. Dr. Nevin Selçuk

Assoc. Prof. Deniz Üner

Dr. Olcay Oymak

ABSTRACT

MATHEMATICAL MODELING OF SULFUR RETENTION IN FLUIDIZED BED COMBUSTORS

Altındağ, Hakan

M.S., Department of Chemical Engineering

Supervisor: Prof. Dr. Nevin Selçuk

Co-Supervisor: Dr. Olcay Oymak

August 2003, 106 Pages

A considerable number of modeling studies for the investigation of sulfur retention in atmospheric bubbling fluidized bed combustors have been carried out and well documented in the literature. Despite 30 years of intensive study of sulfation process in fluidized bed combustors and numerous laboratory studies, there are still many uncertainties and disagreements on the subject. In addition, modeling sulfur retention performance of Turkish lignites with high sulfur, volatile matter and ash contents has not drawn much attention to date. Recent trend in utilization of indigenous lignites in fluidized bed boilers necessitated investigation

of pollutant emissions and adaptation of fluidized bed combustion technology to these lignites. In an attempt to achieve this objective, a system model, previously developed and tested for the prediction of the combustion behavior of fluidized bed combustors was extended to incorporate sulfur retention.

The predictive accuracy of the model was assessed by applying it to the prediction of the behavior of METU 0.3 MW_t ABFBC test rig burning indigenous lignites in their own ashes, and comparing its predictions with measurements taken on the same rig. Sulfur dioxide concentration predictions throughout the combustor were found to be in good agreement with the experimental data except for the small discrepancy between predictions and measurements in the bed section. Measurements and model predictions revealed that recyling enhances calcium utilization significantly by increasing the sorbent residence time leading to higher sulfur retention efficiencies. The system model proposed in this study proves to be a useful tool in qualitatively and quantitatively simulating the processes taking place in an atmospheric fluidized bed combustor.

Keywords: Sulfur retention, fluidized bed combustion, lignite, recycle.

ÖZ

AKIŞKAN YATAKLI YAKICILARDA KÜKÜRT TUTUNUMUNUN MODELLENMESİ

Altındağ, Hakan

Yüksek Lisans, Kimya Mühendisliği Bölümü

Tez Yöneticisi: Prof. Dr. Nevin Selçuk

Yardımcı Tez Yöneticisi: Dr. Olcay Oymak

Ağustos 2003, 106 Sayfa

Kabarcıklı akışkan yataklarda kükürt dioksit tutunumunu araştırmak için çok sayıda modelleme çalışması yapılmış ve literatürdeki yerini almıştır. Ancak, son 30 yılda kabarcıklı akışkan yataktaki kükürt tutunumunu incelemek için yapılan yoğun araştırmalara ve sayısız laboratuvar çalışmalarına rağmen, hala bu konu üzerinde belirsizlikler ve uzlaşmazlıklar sürmektedir. Ayrıca, yüksek kükürt, uçucu madde ve kül içeriğine sahip olan Türk linyitlerinin kükürt tutunumu performansının modellenmesi gerekli ilgiyi görmemiştir. Günümüzde, bu linyitlerin akışkan yataklı kazanlarda kullanımına yöneliş, bu teknolojinin Türk linyitlerine uyarlanmasını ve kirletici gazların emisyonlarının araştırılmasını gerektirmektedir. Bu hedefe ulaşabilmek için, akışkan yataklı yakıcıların yanma davranışlarının öngörülmesi

için geliştirilmiş ve test edilmiş olan bir sistem modeli kükürt tutunumunu içeren bir model haline getirilmiştir.

Model öngörülerinin doğruluğu kendi külü içinde linyit yakan ODTÜ 0.3 MW_t atmosferik kabarcıklı akışkan yataklı yakıcı test ünitesinin davranışının belirlenmesine uygulanmış ve aynı test ünitesi üzerinden alınan ölçümlerle yapılan karşılaştırma ile değerlendirilmiştir. Yatak kısmındaki model öngörüleri ve ölçümler arasındaki küçük bir fark dışında yakıcı boyunca kükürtdioksit konsantrasyonu öngörülerinin deneysel verilerle uyum içerisinde olduğu görülmüştür. Ölçümler ve model öngörüleri geri döngünün kireçtaşının yatakta kalma süresini artırarak kasiyum kullanımını önemli ölçüde artırdığını ve bunun da daha yüksek kükürt tutunumu veriminin elde edilmesini sağladığını göstermiştir. Bu çalışmada önerilen sistem modelinin akışkan yataklı yakıcıda gerşekleşen olayların nicel ve nitel temsilinde yararlı olduğu görülmüştür.

Anahtar kelimeler: Kükürt tutunumu, akışkan yataklı yakıcı, linyit, geri döngü.

to *Züm*

ACKNOWLEDGEMENTS

I would like to express my deepest gratitude to my supervisor, Prof. Dr. Nevin Selçuk for her guidance and constant encouragement throughout this study.

I would like to show my appreciation to my co-supervisor Dr. Olcay Oymak, for his precious suggestions and support.

I also thank to the AFBC research team members for their friendship and support during my study; Yusuf Göğebakan, Hakan Harmandar, Aykan Batu, Tanıl Tarhan, Işıl Ayrancı, Ahmet Bilge Uygur and Semra Harmandar. I owe particular thanks to my colleagues Hakan and Yusuf, for their outstanding help and patience.

My Special thanks go to my family for their great support, encouragement and unshakable faith in me.

Financial support provided by Middle East Technical University (METU) through BAP-2003-07-02-00-11 project is gratefully acknowledged.

Finally, a debt of my warmest thanks goes to my wife, Zümrüt, for understanding my frequent absences and for her endless patience and encouragement when it was most required.

TABLE OF CONTENTS

LIST OF TABLES

LIST OF FIGURES

LIST OF SYMBOLS

a	Decay constant, cm^{-1}
A	Cross-sectional area, cm^2
Ar	Archimedes number, -
c_p	Specific heat capacity, $cal\ g^{-1}\ K^{-1}$
C	Concentration, $mol\ cm^{-3}$
d	Diameter, cm
D	Diffusivity of oxygen in nitrogen, $cm^2\ s^{-1}$
E	Activation energy, $cal\ mol^{-1}$
$E(r)$	Elutriation rate constant, s^{-1}
$E(t)$	Solids residence time distribution function
$f(E)$	Activation energy distribution function for devolatilization, $mol\ cal^{-1}$
F	Char flow rate, $g\ s^{-1}$
F_z	Upward flow rate of entrained particles at any height z in freeboard, $g\ s^{-1}$
g	Gravitational acceleration, $cm\ s^{-2}$
h	Individual heat transfer coefficient, $cal\ cm^{-2}\ s^{-1}\ K^{-1}$
H	Height, cm
ΔH^0	Heat of reaction at standard state, $cal\ mol^{-1}$
k	Overall sulfation rate constant, cm/s; thermal conductivity, $cal\ cm^{-1}\ s^{-1}\ K^{-1}$
$k(E)$	First-order reaction rate constant for devolatilization, s^{-1}
k_C	Reaction rate constant for char combustion, $cm\ s^{-1}$
k_{CO}	Reaction rate constant for CO oxidation, $(cm^3\ mol^{-1})^{0.8}\ s^{-1}$

k_f	Film mass transfer coefficient, $cm\ s^{-1}$
k_s	First order surface reaction rate constant for char combustion, $cm\ s^{-1}$; first order kinetic rate constant for sulfation reaction, $cm\ s^{-1}$
K_{be}	Interphase mass transfer coefficient, s^{-1}
$K^*_{i\infty}$	Dispersed non-cluster flux of entrained particles in size i, $g\ cm^{-2}\ s^{-1}$
K^*_{ih}	Cluster flux of entrained particles in size i, $g\ cm^{-2}\ s^{-1}$
K^*_i	Total flux of entrained particles in size i, $g\ cm^{-2}\ s^{-1}$
L	Length, cm
m	Mass flow rate, $g\ s^{-1}$
M	Molecular or atomic weight, $g\ mol^{-1}$; hold-up in the bed, g
n	Index of the dimension; molar flow rate, $mol\ s^{-1}$
n_C	Carbon consumption rate, $mol\ cm^{-3}\ s^{-1}$
N_r	Number of cycles of recycled sorbent and ash particles
$P(r)$	Size distribution function, cm^{-1}
$P_z(r)$	Size distribution of entrained particles at any height z in freeboard, cm^{-1}
Q	Volumetric flow rate, $cm^3\ s^{-1}$; energy generation/loss rate, $cal\ s^{-1}$
q_s	Calcium oxide concentration on the sorbent surface, $mol\ cm^{-2}$
r	Spatial independent variable, cm
r_C	Carbon consumption rate on the surface of char particle, $mol\ cm^{-2}\ s^{-1}$
r_{CO}	Rate of CO combustion, $mol\ cm^{-3}\ s^{-1}$
r_{SO_2}	Rate of sulfation reaction, $mol\ s^{-1}$
R	Ideal gas constant, $cal\ mol^{-1}\ K^{-1}$; radius, cm
$\boldsymbol{R}$	Energy generation/loss rate in freeboard, $cal\ cm^{-3}\ s^{-1}$
$\Re$	Species generation/depletion rate, $mol\ cm^{-3}\ s^{-1}$
$\Re(r)$	Shrinkage rate of char particles, $cm\ s^{-1}$
Re_p	Particle Reynolds number, -
R_w	Thermal resistance across the freeboard wall, $cal\ cm^{-2}\ s^{-1}\ K^{-1}$
S	External sorbent surface area, cm^2
t	Time, s
T	Temperature, K
u_0	Superficial velocity in the bed, $cm\ s^{-1}$

u_b	Superficial bubble phase velocity, $cm\ s^{-1}$
u_e	Superficial velocity in emulsion phase, $cm\ s^{-1}$
u_{mf}	Superficial minimum fluidization velocity, $cm\ s^{-1}$
u_t	Terminal velocity of the particles, $cm\ s^{-1}$
u_{tf}	Superficial throughflow velocity in bubbles, $m\ s^{-1}$
U	Overall heat transfer coefficient, $cal\ cm^{-2}\ s^{-1}\ K^{-1}$
U_f	Unit filter function
v	Volatiles released, %
v_∞	Ultimate yield of volatiles released, %
V	Volume, cm^3
x	Mass fraction (dry basis); spatial independent variable, cm
x_{vl}	Fraction of volatiles released in the bed
y	Mole fraction
z	Spatial independent variable, cm

Greek Letters

α	Thermal diffusivity, $cm^2\ s^{-1}$
δ	Bubble phase volume fraction
ε	Voidage; emissivity; convergence criterion
ε_f	Voidage at fluidization conditions
ε_{mf}	Voidage at minimum fluidization conditions
ε_s	Solids volume fraction
η	Contact efficiency
λ^0	Latent heat of vaporization at standard state, $cal\ g^{-1}$
μ	Viscosity, $g\ cm^{-1}\ s^{-1}$
ρ	Density, $g\ cm^3$
σ	Standard deviation of activation energy distribution, $J\ mol^{-1}$; Stephan-Boltzman constant, $cal\ cm^{-2}\ s^{-1}\ K^{-4}$; Fractional sorbent surface area
τ	Residence time, s^{-1}
ϕ	Sphericity, -

Subscripts

32	Surface/volume mean
a	Air; ash; attrition
avg	Average
b	Bubble
bd	Bed drain
bed	Bed
bw	Bed wall
c	Combustion
C	Carbon
co	Carryover
cw	Cooling water
d	Char
e	Emulsion
elut	Elutriation
f	Freeboard; fine; feed coal
fc	Fixed carbon
fw	Freeboard wall
G	Gas
H	Hydrogen
I	Inert; inner
J	Species index
lst	Limestone
max	Maximum
maxe	Maximum elutriated
min	Minimum
o	Feed; outer; at the bed surface; initial
p	Particle
r	Radiation; reference
recy	Recycle
rxn	Reaction
S	Sulfur

s	Surface; solid
T	Tube
vm	Volatile matter
w	Wall; water

Abbreviations

FBC	Fluidized Bed Combustion
ABFBC	Atmospheric Bubbling Fluidized Bed Combustor
AFBC	Atmospheric Fluidized Bed Combustor

CHAPTER 1

INTRODUCTION

Advantages of Fluidized Bed Combustion (FBC) technology such as the ability to burn wide variety of fuels efficiently and to control pollutant emissions without flue gas treatment systems have led to a steady increase in its commercial use over the past decades. FBC allows clean combustion of low-grade coals with in-situ retention of sulfur dioxide (SO_2) produced in burning such coals by the addition of either limestone or dolomite as sorbent.

In Turkey there exist widely spread lignite reserves with an estimated total quantity of 8 billion tons. A major proportion of this quantity is characterized by high sulfur, volatile matter and ash contents. Therefore, it is difficult to achieve clean and efficient combustion of these low calorific value lignites in conventional combustion systems. Always more demanding environmental regulations make it necessary to retrofit to conventional power generation facilities with a flue gas desulfurization unit for removal of SO_2. Although acceptable results have eventually been achieved in most cases, these have been at the cost of considerable

delays in project start-up, high capital investment, stringent operational vigilance, and frequent and expensive maintenance and repair. FBC technology offers the industry and utilities an alternative method of utilizing indigenous lignites in an efficient and environmentally acceptable manner as confirmed by the results of extensive research carried out on combustion and in-situ desulfurization characteristics of these lignites in pilot scale fluidized bed combustors [1-15, 91]. However, combustion and emission performance of Turkish lignites has not yet been fully investigated. A limited number of sulfur retention modeling studies [13, 16] have been carried out to date on SO_2 emissions from bubbling fluidized bed combustion of these high sulfur containing lignites with simplifying assumptions such as negligible freeboard sulfur capture or average sorbent particle diameter representing wide size distribution. In none of these studies SO_2 concentration profile throughout the combustor was predicted and validated against experimental data. Moreover, there is no sulfur retention modeling study on these indigenous lignites with recycling of elutriated particles from the combustor. Therefore, absence of a reliable model to fulfill the goal of optimal design and operation of fluidized bed combustors burning indigenous lignites in their own ashes on one hand, and recent trend in utilization of local reserves in industry and utility boilers on the other, necessitated the investigation of sulfur capture performance of fluidized bed combustors by developing a model and testing its predictions against experimental data obtained from 0.3 MW_t Atmospheric Bubbling Fluidized Bed Combustor (ABFBC).

In order to investigate the sulfur retention in fluidized bed combustion systems a system model, originally proposed by Selçuk and Sivrioğlu [17] and later improved, extended and validated against experimental data by Selçuk and her

colleagues [5, 9, 11, 13, 16, 18-33], was chosen as a basis for the incorporation of sulfur retention. The system model in its original form accounts for bed and freeboard hydrodynamics, volatiles release and combustion, char particles combustion and size distribution, attrition and heat transfer but excludes sulfur retention.

Therefore, objectives of the present study have been to

- extend the existing code for ABFBC simulation for incorporation of sulfur retention sub-model,
- perform combustion tests with limestone addition at different recycle ratios on a 0.3 MW_t ABFBC Test Rig burning Turkish lignites in their own ashes for the determination of sulfur retention characteristics,
- validate the model predictions against experimental data.

CHAPTER 2

SULFUR RETENTION MODELING IN ABFBC

In the past three decades, a considerable number of modeling studies have been carried out to investigate the sulfur retention in atmospheric bubbling fluidized bed combustors. Therefore, this technology is frequently viewed as a mature technology that does not require additional basic insights to achieve effective sulfur removal. However, despite 30 years of intensive study of sulfation process in ABFBC and numerous laboratory studies, there are still many uncertainties and disagreements on the subject. In addition, gradual introduction of increasingly restrictive legislations on emissions from combustion sources has been keeping the topic attractive for further research. At present, many mathematical models on sulfur retention in ABFBC are available. Tables 2.1 and 2.2 are arranged to give a quick insight into these models. Table 2.1 summarizes the studies on sulfur retention modeling in the open literature and Table 2.2 describes the nomenclature used in Table 2.1.

Table 2.1 Summary of studies on sulfur retention modeling in the open literature.

Author(s)	Year	A	B	C	D	E	F	G	H	I	J	K
Bethell et al. [34]	1973	1	1	2/Yes	3+5	2	Yes/2	No	2	1	1	No
Chen & Saxena [35]	1977	3	1	2/Yes	3+5	2	Yes/2	No	2	1+2a	1	Yes
Rajan et al. [36]	1978	2a	2	2/Yes	4+5	1a	Yes	No	2	1+2a	1	Yes
Rajan &Wen [37]	1980	2a	2	2/Yes	4+5	1a	Yes	Yes	2	1+2b	1	Yes
Lee et al. [38]	1980	2b	3	1/No	3	2	No	No	1	1	1	No
Lee & Georgakis [39]	1981	2b	3	1/No	2	2+3b	No	No	1	1	1	No
Zheng et al. [40]	1982	2b	3	1/No	5	2	No	No	1	1	1	No
Fee et al. [41]	1983	2b	3	1/No	2	2	No	No	1	1	1	No

Table 2.1 Summary of studies on sulfur retention modeling in the open literature (continued).

Author(s)	Year	A	B	C	D	E	F	G	H	I	J	K
Fee et al. [42]	1984	2b	3	1/No	1	2	No	Yes	1	1	1	No
Ho et al. [43]	1986	2b	1	1/No	5	1a	No	No	2	1	3	No
Hodges et al. [44]	1987	2	3	1/Yes	5	2	Yes/2	Yes	1	1	1	Yes
Schouten & van den Bleek [45, 46]	1987 & 1988	2b	3	1/No	5	2+4	No	No	1	1	1	No
Dennis & Hayhurst [47, 48]	1986 & 1988	2b	3	1/Yes		1b	Yes	Yes	2	1	1	No
Zhang et al. [49]	1989	1	1	2/No	2	2	No/2	No	1	1+2b	1+2	No
		1	1	2/No	1	2	No/2	No	1	1+2b	1+2	No
		1	2	2/No	1	2	No/2	No	1	1+2b	1+2	No

Table 2.1 Summary of studies on sulfur retention modeling in the open literature (continued).

Author(s)	Year	A	B	C	D	E	F	G	H	I	J	K
Lin et al. [50, 51]	1990 & 1991	1	2	2/No	5	2+4	No/2	No	1	1	1	No
Rubiera et al. [52]	1991	2b	3	1/Yes	2	2+4	Yes/2	No	1	1	1	No
Lin et al. [53, 54]	1992 & 1993	1	2	1/No	5	1b	No	No	1	1	1	No
Selçuk et al. [16]	1993	2b	1	1/No	2	2+4	No	No	1	1	1	Yes
Walsh [55]	1995	2	1	2/No	2	2+4	Yes/2	Yes	1	1	1	No
Huilin et al. [56]	1999	3	1	No		2+4			1	1+2a	3	Yes
Degirmenci et al. [13]	2000	2b	1	1/No	4	2+4	No	No	1	1	1	Yes

Table 2.2 Nomenclature for Table 2.1.

A. Fluid Bed Model:

1. One phase model.
2. Two phase model.
    a. Two phase bubbling bed model, clouded bubbles; bubble and emulsion phase; bubble size dependent on bed height; gas exchange between bubble and emulsion phases axially distributed.
    b. Two phase bubbling bed model; bubble phase and emulsion phase; average bubble size; average gas exchange coefficient.
2. Three phase bubbling bed model; bubble, cloud-wake and emulsion phase; bubble size dependent on bed height; gas exchange between phases based on average bubble volume.

B. Gas Flow Pattern:

1. Plug flow in all phases.
2. Mixed flow in all phases.
3. Well mixed in the emulsion phase; plug flow in the bubble phase.

C. Sorbent Flow In The Bed :

1. Well mixed in the emulsion phase.
2. Well mixed
3. Size distribution considered: Yes/No

Table 2.2 Nomenclature for Table 2.1 (continued).

D. Sulfur Release:

1. Sulfur released at the base of the bed.
2. Sulfur release uniform throughout the bed.
3. Sulfur release not uniform throughout the bed.
4. Sulfur release during devolatilization considered.
5. Sulfur release rate proportional to char combustion rate.

E. Sulfur Capture:

1. Sulfation kinetics model
    a. Grain model.
    b. General gas-solid volume reaction model with structural change of particle.
2. Semi-empirical sulfur capture kinetic equation.
3. Sulfation rate proportional to external sorbent surface area.

F. Elutriation:

1. Sorbent elutriation considered: Yes/No
2. Recirculation of elutriated particles.

G. Freeboard:

1. Freeboard sulfur retention considered: Yes/No

Table 2.2 Nomenclature for Table 2.1 (continued).

H. Model Complexity:

1. Simple analytical expressions.
2. More complex (numerical) calculations.

I. Model Predictions:

1. Sulfur retention efficiency.
2. SO_2 concentration profile.
    a. SO_2 concentration profile along the bed.
    b. SO_2 concentration profile along the combustor.

J. Model Test:

1. Sulfur retention efficiency validated against experimental data.
2. SO_2 concentration profile validated against experimental data.
3. No validation.

K. Comprehensive Overall Model:

Sulfur retention model incorporated into a comprehensive overall model: Yes/No

As displayed in Table 2.1 and Table 2.2, major factors determining sulfur retention include:

1. The sulfation kinetics model.
2. Hydrodynamics in the bed, which determines the gas mixing.
3. The mixing of solid particles.
4. The particle size distribution of the sorbent.
5. The elutriation and recirculation of the sorbent.
6. The release pattern of the sulfur content, which may be coupled with the devolatilization and combustion processes.

The published models for sulfur capture may be classified into two general categories: comprehensive (such as the grain or pore volume reaction model) [36, 37, 43, 47, 48, 53, 54] and semi-theoretical [13, 16, 34, 35, 38-42, 44, 45, 49-52, 55, 56]. Due to the complex nature of the phenomena, a comprehensive gas solid reaction model usually includes a set of equations containing a large number of parameters, which have to be specified by empirical correlations or sometimes estimated theoretically. One of the disadvantages of a detailed gas-solid reaction model as mentioned by Lee and Georgakis [39], Fee *et al.* [41], Dennis and Hayhurst [48], Schouten and van den Bleek [45], Zhang *et al.* [49] and Lyngfelt *et al.* [57] is that it takes into account changes of structural solid properties, which are highly non-linear. Therefore, it is rather difficult to incorporate them into fluid dynamic models of fluidized bed combustors without resorting to excessively long computer calculations, which limits their use in FBC. Although such models provide a good understanding of the sulfation process, such a rigorous analysis of the sulfation reaction may result in too complex mathematical expressions for

practical application in design or data correlation. Another disadvantage is that these models require thorough knowledge of particle properties such as pore size distribution and grain diameters that are strongly stone dependent. In addition to that, physical constants such as effective solids diffusion coefficient, which are extremely difficult to determine experimentally, are required. Most of the time these constants are obtained by adjusting them according to experimental data. However, it must be admitted that despite these disadvantages, the mechanistic models contribute to the basic understanding of the influence of the solids structure on the overall reaction rate.

To avoid the possible extensive computation as well as the problem of experimental determination of physical constants and solid properties, a more recent trend in fluidized bed modeling of sulfur retention is based on the experimental observation that the decay in the overall sorbent conversion can easily be fitted by an exponential, reciprocal or other type of empirical relation. For instance, Zheng *et al.* [40] followed this approach by using the analogy between particle sulfation and catalyst deactivation, which is conventionally described in terms of the exponential decrease in the available surface area with time. This enables the description of the system in terms of two time-invariant rate constants, one characterizing the initial surface reaction and the other the observed exponential decrease in sorbent activity with time. Motivated by the experimental observations that the reaction rate decreases with time in an exponential fashion, Lee and Georgakis [39] proposed an expression to describe the overall sulfation reaction rate. The semi-emprical simplified rate expression proposed for the sulfation reaction characterizes the gas-solid reaction by two parameters, namely the sulfation time and the pore plugging constant. The sulfation time is a measure of the chemical reactivity of the stone with

the effect of diffusional resistance taken into consideration. The pore plugging constant is a measure of the stone's ability to accommodate the volume of reaction product accumulated in the pores. Another semi-empirical model developed by Schouten and van den Bleek [45], provides an analytical expression for the calcium to sulfur (*Ca/S*) ratio as a function of sulfur retention, maximum calcium oxide (*CaO*) utilization and two dimensionless model parameters: a retention parameter and a two-phase gas flow parameter. The former parameter is calculated from combustor conditions and sorbent properties while the latter is a function of the number of gas transfer units and dimensionless excess gas velocity. In a more recent study, Rubiera *et al.* [52] developed a two parameter semi-empirical model. Similar to the model proposed by Zheng *et al.* one parameter characterizes the initial fast reaction rate while the other is a measure of the ultimate sulfation capacity of the stone. The use of semi-empirical approach to describe the complicated kinetics of sulfation reaction is one of the most widely preferred methods especially in the modeling of sulfur retention in bubbling fluidized bed combustors.

Similar to comprehensive gas-solid reaction models that take into account structural changes of the sorbent during the course of the reaction, semi-theoretical models also include the effects of physical and chemical mechanisms. However, for the sake of simplicity, the processes in the bed are not described in detail, which makes it easier to incorporate sulfation kinetics into fluid dynamical model of the combustor. The fluidized bed combustor is usually treated as a reactor or a series of reactors with appropriate assumptions for solids mixing, flow pattern and the location of sulfur release. Therefore, analytical solutions for semi-theoretical models are relatively easy to obtain.

A number of standard assumptions are made in modeling hydrodynamics of ABFBC systems. The bed is assumed to be formed by one or two phases and the gas is in plug flow or well mixed. The choice of the type of fluid dynamical reactor model is strongly dependent on the mode of fluidization and gas transport. If the interstitial gas velocity exceeds the bubble rising velocity, the fluidizing gas uses the bubbles as a shortcut on its way through the bed. Therefore, there is a little difference in gas concentrations between bubble and emulsion phases and a one-phase model can more closely approximate the bed. For this reason, Bethell *et al.* [34], Zhang *et al.* [49] and Lin *et al.* [50, 51, 53, 54] developed one-phase models by using this approach. However, in most of the studies the opposite case is valid and the bubbling bed is viewed as consisting of two phases; a dilute or bubble phase composed of solids free gas in plug flow and a dense or emulsion phase, consisting of the solid particles and a volume of gas called interstitial, which is well stirred [13, 16, 36-47, 52, 55]. In addition, Chen and Saxena [35] and Huilin *et al.* [56] applied a three-phase model to represent bed hydrodynamics. This model assumes that bubbles, whilst moving up, drag solid particles in their wake. The upflow of solids in the wake phase is balanced by downflow of solids in the emulsion phase and there is a continuous exchange of solids between the wake and emulsion phases. Nevertheless, this model has not been used so widely due to its complex description of the bed hydrodynamics.

Solid mixing and particle size distribution of the sorbent are two other important aspects of the physical process that must be incorporated into a model. The solid mixing pattern depends on how the characteristic reaction time compares with the time period required for a solid particle to travel a distance comparable to the dimensions of the bed. Since the time of sulfation and char combustion are one

to two orders of magnitude higher than that of mixing, the generally accepted assumption of well mixed particles is reasonable. However, various approaches are preferred by different researchers with respect to sorbent size distribution. In some of the studies [13, 16, 38-43, 45, 49-51, 53-56] sorbent particle size distribution is not considered and it is assumed that sulfur capture performance of the sorbent with a wide size distribution is equivalent to the performance of the same amount of sorbent with a specific size which is defined as the effective sorbent particle size in the bed. Although this assumption greatly simplifies the calculations, it is not realistic because available surface area depends on the particle size. For this reason, it is more logical to take sorbent particle size distribution into account.

Determination of sorbent particle size distribution also makes it possible to find out the amount of sorbent entrained to the freeboard or elutriated from the combustor. The loss of fines by elutriation is a drawback for the efficient sulfur capture and should be considered in the model. The freeboard sulfur capture was taken into account for the first time by Rajan and Wen [37] and later a model indicating the importance of freeboard sulfur capture was proposed by Fee *et al.* [42]. For an overall sulfur retention of 90 %, approximately 9 % of the sulfur was predicted to be captured within the freeboard above a combustor bed 1.8 m by 1.8 m by 1.2 m high of 1200 μm diameter limestone particles that are fluidized at 2.4 m/s. They also conclude that the sulfur captured by the entrained particles is negligible. This conclusion was also confirmed by Dennis and Hayhurst [47], who tried two cases with and without sulfur capture by entrained particles and observed no significant effect of reaction in the freeboard concerning entrained particles.

In order to compensate for the loss of sulfur capture efficiency due to elutriation of fine sorbent particles from the combustor, recycling may be used. The

number of studies on sulfur retention modeling with recycle of elutriated sorbent particles is very limited. Hodges *et al.* [44] investigated the effect of recycle ratio on the sulfur retention efficiency and observed that recycling increases calcium utilization by increasing the residence time of elutriated sorbent particles. Rubiera *et al*. [52], on the other hand, studied the effect of recycle ratio on the sulfur capture parametrically. On the basis of the parametric study they concluded that up to a recycle ratio of 0.9 sulfur retention efficiency increases and reaches a maximum. However, according to their model, further increase in recycle ratio causes an adverse effect on the sulfur capture efficiency, which was not explained clearly by the authors. A more recent study was performed by Walsh [55] on the sulfur retention modeling with recycle. According to experiments carried out at a 20 MW ABFBC, the *Ca/S* ratio required for 90 % sulfur capture was found to decrease with increasing recycle ratio. However, in contrast to experimental observations, the *Ca/S* ratio required for 90 % sulfur capture was predicted to be independent of recycle ratio due to the underestimation of the contribution of recycled fines to sulfur capture in the model.

As for the sulfur release pattern, various approaches have been developed. It is clear that under oxidizing circumstances in the bed the sulfur is predominantly released in the form of SO_2, which originates from the combustion of the sulfur content of the coal. Bethell *et al.* [34] assumed that all the sulfur was released at the bottom of the bed or uniformly throughout the bed, consequently, they observed that the latter assumption was in better agreement with the experimental data. Zhang *et al.* [49], on the contrary, reached an opposite conclusion upon validating their model against experimental data. Alternatively, since much of the sulfur content of the coal is contained in the volatiles, sulfur release may be coupled with

the volatiles release pattern [13, 36, 37, 50, 51]. In a very recent study [58] experiments were performed at a 0.3 MW_t ABFBC without limestone addition with a lignite containing negligible amount of inherent *CaO* content in order to observe the release pattern of SO_2 in the absence of sulfur capture. SO_2 concentration was found to increase continuously throughout the combustor and levels off toward the exit. This was attributed to the progressive release of volatiles throughout the combustor, which implies the necessity of sulfur capture up in the freeboard.

The published models in the open literature generally predict the sulfur retention efficiency as a function of operating conditions such as fluidizing velocity, *Ca/S* and recycle ratios. However, the number of studies for the prediction of SO_2 concentration profiles hence the sulfur release throughout the combustor is very limited [37, 49]. Among these studies only Zhang *et al.* [49] validated the SO_2 concentration predictions of the model against experimental data. Prediction of SO_2 concentration along the combustor makes it possible to determine the sections of the combustor where SO_2 concentration is higher. Therefore, operating conditions can be arranged to achieve additional sulfur capture in these regions. For instance, higher SO_2 concentrations in the freeboard shows the necessity of recycling to increase the amount of sulfur captured in the freeboard. A comparison between SO_2 concentration profile predictions and measurements is also crucial in the sense that it reveals how realistic the model describes the physical and chemical phenomena taking place in the combustor.

CHAPTER 3

STEADY-STATE ABFBC MODEL WITH IN-SITU DESULFURIZATION

A system model, originally proposed by Selçuk and Sivrioğlu [17] and later improved, extended and validated against experimental data by Selçuk and her colleagues [5, 9, 13, 16, 18-33, 59], was chosen as a basis for incorporation of desulfurization. It is developed on the basis of first principles and used to correlate data from METU 0.3 MW ABFBC Test Rig. The system model in its present form accounts for bed and freeboard hydrodynamics, volatiles release and combustion, char particles combustion and size distribution, heat transfer and attrition but excludes desulfurization.

The behavior of the fluidized bed combustor under consideration is described by a model based on conservation equations for energy and chemical species in conservative form for both bed and freeboard sections. The assumptions involved are illustrated in Figure 3.1 and Figure 3.2 for the bed and freeboard sections, respectively. The correlations used in estimating important parameters in

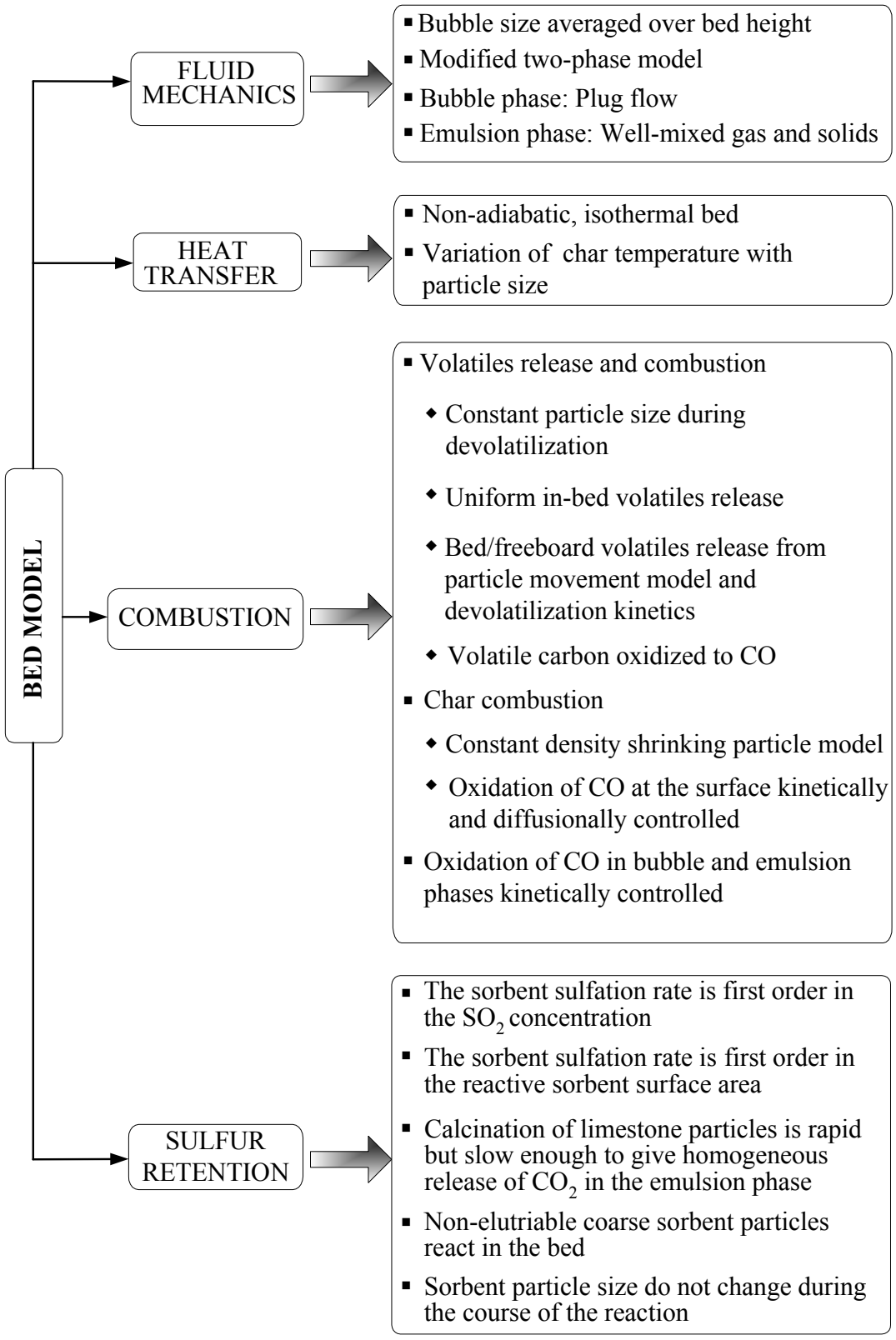

Figure 3.1 An overview of the steady state bed model assumptions.

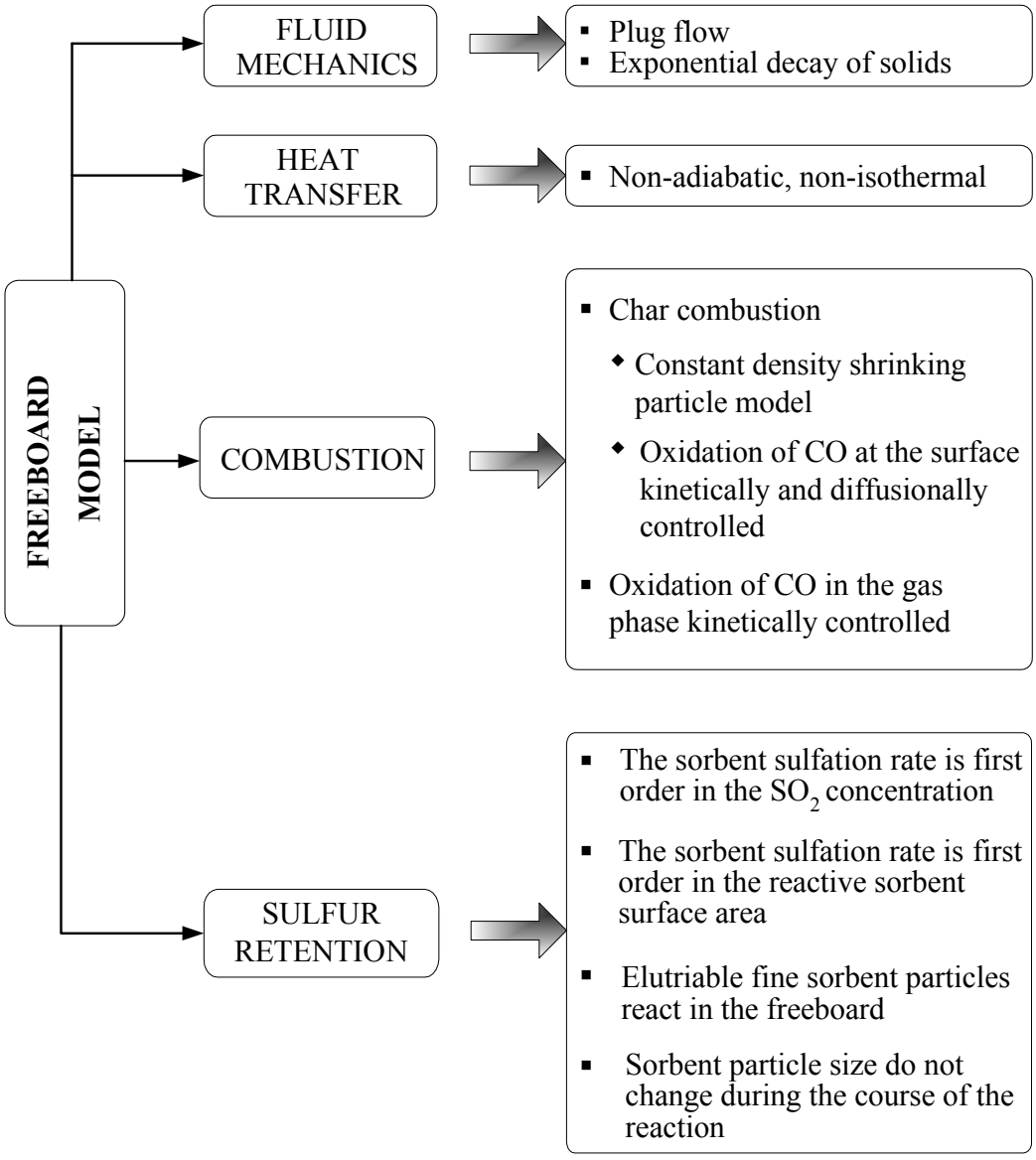

Figure 3.2 An overview of the steady state freeboard model assumptions.

the model are listed in Table 3.1. Chemical reactions included in the model together with their rate expressions are given in Table 3.2. Details of the model without desulfurization can be found elsewhere [60]. However, for the sake of integrity, the sub-models utilized are described in the following sections.

Table 3.1 Correlations used in the model.

	Reference
Mass transfer to particles in the emulsion phase, k_f	[61]
Heat transfer to particles in the emulsion phase, h_p	[62]
Specific elutriation rate constant, $E(r)$	[63]
Terminal velocity of the particles, u_t	[64]
Bubble to emulsion mass transfer, K_{be}	[65]
Minimum fluidization velocity, u_{mf}	[66]
Bubble size, d_b	[67]
Emulsion phase velocity, u_e	[68]
Bubble phase volume fraction, δ	[68]
Convective heat transfer coefficient of bed wall, h_{bw}	[64]
Convective heat transfer coefficient of cooling tubes, h_{cw}	[69]
Convective heat transfer coefficient of cooling water, h_i	[70]
Exponential decay constant, a	[63]
Gas side heat transfer coefficient in freeboard, h_g	[62]

Table 3.2 Reactions and rate expressions.

#	Reaction	Place	Rate expression	Parameters	Reference
1	$C_s + 1/2O_2 \rightarrow CO$	Char surface	$k_c C_{O_2\,s}$	$k_C = -5.95 \times 10^4 T_p \exp(-17967 / T_p)$	[71]
2	$C + 1/2O_2 \rightarrow CO$	Gas phase	Instantaneous	-	-
3	$CO + 1/2O_2 \rightarrow CO_2$	Gas phase	$k_{CO} C_{O_2}^{0.3} C_{CO} C_{H_2O}^{0.5}$	$k_C = -3.0 \times 10^{10} T \exp(-8052 / T_g)$	[72]
4	$H_2 + 1/2O_2 \rightarrow H_2O$	Gas phase	Instantaneous	-	-
5	$S + O_2 \rightarrow SO_2$	Gas phase	Instantaneous	-	-
6	$CaCO_3 \rightarrow CaO + CO_2$	Sorbent particle	Instantaneous	-	-
7	$CaO + SO_2 + 1/2O_2 \rightarrow CaSO_4$	Sorbent surface	$k C_{SO_2} S$	-	-

3.1 Bed Model

Bed model can be described in terms of bed hydrodynamics, volatiles release and combustion, char combustion, particle size distribution of bed char and bed char holdup and desulfurization.

3.1.1 Bed Hydrodynamics

Bed hydrodynamics is based on modified two-phase theory suggested by Grace and Clift [73],

$$u_o = \frac{Q_b}{A_{bed}} + u_{tf} + u_e(1-\delta) \tag{3.1}$$

where throughflow velocity, u_{tf}, can be expressed in terms of emulsion phase velocity, u_e, using modified n-type two-phase theory of Grace and Harrison [74],

$$u_{tf} = (n+1)u_e\delta \tag{3.2}$$

where $n = 2$ for three dimensional beds. Gas/solids in the emulsion phase and gas in the bubble phase are assumed to be well-stirred and in plug flow, respectively. Minimum fluidization velocity can be obtained from Ergun equation [66]:

$$\frac{1.75}{\varepsilon_{mf}^3\phi_s}\left(\frac{d_p u_{mf}\rho_g}{\mu}\right)^2 + \frac{150(1-\varepsilon_{mf})}{\varepsilon_{mf}^3\phi_s^2}\left(\frac{d_p u_{mf}\rho_g}{\mu}\right) = \frac{d_p^3\rho_g(\rho_i-\rho_g)g}{\mu^2} \tag{3.3}$$

An integrated average mean bubble size found from bubble size expression proposed by Mori and Wen [67], in the sections unoccupied by the tube bank and from constant and uniform bubble size determined by the clearance between the tubes is utilized. Bubbles are assumed to be free of solids. The gas interchange

coefficient between bubble and emulsion phases is defined as:

$$K_{be} = \frac{\left(\begin{array}{c} volume\ of\ gas\ going\ from\ bubbles \\ to\ emulsion\ or\ from\ emulsion\ to\ bubbles \end{array} \right)}{\left(volume\ of\ bubbles\ in\ the\ bed \right)\left(time \right)} \tag{3.4}$$

In this thesis study, the following relationship was used for K_{be} [65],

$$K_{be} = 7.14\frac{u_e}{d_b} + 5.46\frac{D^{1/2}}{g^{1/4}d_b^{5/4}}\frac{\varepsilon_{mf}}{1+\varepsilon_{mf}} \tag{3.5}$$

This is a modified Davidson-Harrison [75] equation put forward to allow for the observation that bubbles in a real fluid move faster than was assumed in the original theory. In utilizing Equation (3.5) the second term is neglected since it is approximately two orders of magnitudes smaller than the first term.

The reason behind the choice of the Equation (3.5) instead of the one utilized in the original system model [60] for the prediction of the combustion behavior was its deficiency in the prediction of the speed of gas interchange between the emulsion and bubble phases with respect to SO_2, concentration of which is lower than those of other species. This is also confirmed by the findings of several other studies [65, 76]. Details on the choice of this expression can be found in Appendix A.

3.1.2 Volatiles Release and Combustion

Volatiles are assumed to be released uniformly in the emulsion phase. The amount released in bed is determined by using the volatile release model of Stubington *et al.* [77], and to describe the devolatilization kinetics the parallel independent reaction model of Anthony and Howard [78] is used. In the presence of radial

temperature profile and with the assumption of evenly distributed volatile matter in the particle, total amount of volatile matter released with respect to time is given by:

$$\frac{v_{avg}}{v_{\infty}} = \frac{3}{R^3}\int_0^R \left[1 - \int_0^{\infty} exp\left(-\int_0^t k(E)dt \right) f(E)\,dE \right] r^2 dr \tag{3.6}$$

Devolatilization history of the particle yields the fraction of volatiles released in bed. The remaining volatiles are assumed to be released to freeboard while the particle is at the bed surface. With regard to combustion of volatiles released, volatile carbon and hydrogen are assumed to burn instantaneously to carbon monoxide (*CO*) and water (H_2O), respectively. The oxidation of *CO* takes place in both bubble and emulsion phases according to the rate expression of Hottel *et al.* [72]. Further details of the volatiles release model can be found in [60].

3.1.3 Char Combustion

Char particles are assumed to burn only to *CO*, as it is the major product of char combustion for typical FBC temperatures. Using the shrinking particle model and taking film mass transfer and the kinetics resistance into consideration, the rate of carbon oxidation at the particle surface can be obtained as

$$r_{C,e} = \frac{2}{1/k_f + 2/k_s}\bar{C}_{O_2,e} \tag{3.7}$$

Film mass transfer coefficient, k_f, is obtained from the equation suggested by Jung and La Nauze [61]. Kinetics of combustion of char particles is assumed to be represented by equation of Field *et al*. [71]. Average emulsion phase oxygen (O_2) concentration is used to calculate combustion rate.

3.1.4 Char Particles Size Distribution

Since carbon consumption rate depends on the surface area provided by the burning char particles, calculation of particle size distribution and holdup of char particles is of fundamental importance in the prediction of behavior of ABFBCs.

In order to derive an equation based on the mass fractions in size intervals for shrinking char particles the following assumptions are made:

1. Char particles enter the bed at a rate of F_o with size distribution of $P_o(r)$ which is expressed by Rosin-Rammler size distribution function.
2. As char particles are well-mixed, bed drain char size distribution represents the bed char size distribution:

$$P_{bd}(r) = P_{bed}(r) \tag{3.8}$$

3. The rate of elutriation of char particles of size r is directly proportional to their concentration in the bed, *i.e.*,

$$F_{co}P_{co}(r)dr = M_d P_{bed}(r)E(r)dr \tag{3.9}$$

where $E(r)$ is the elutriation rate constant [63], M_d is the total mass of char in the bed and $P_b(r)$ is the size distribution of char particles in the bed.

4. Carryover char size distribution represents the recycle char size distribution, since both streams are elutriated from the bed:

$$P_{co}(r) = P_{recy} \tag{3.10}$$

5. Densities of char particles do not change during the burn-out.
6. Char particles can be attrited until reaching the upper size limit of the fines,

r_f, and then becomes a fine particle itself. Fines generated by attrition are not attritable themselves.

7. Char particles are considered to shrink by combustion and attrition according to shrinking particle model at a rate of

$$\left(\frac{dr}{dt}\right)=\left(\frac{dr}{dt}\right)_c+U_f\left(r_{max},r_f\right)\left(\frac{dr}{dt}\right)_a \tag{3.11}$$

where U_f is unit filter function defined to differentiate particle size ranges attained due to both combustion and attrition and due to combustion only. A detailed discussion on definition of unit filter function can be found elsewhere [79].

The steady state population balance on mass basis on char particles in the interval $r + \Delta r$ can be stated in verbal form as,

$$\begin{Bmatrix}Char\ Entering\\ in\ feed\end{Bmatrix}+\begin{Bmatrix}Char\ entering\\ in\ recycle\end{Bmatrix}-\begin{Bmatrix}Char\ leaving\\ in\ bed\ drain\end{Bmatrix}-\begin{Bmatrix}Char\ leaving\\ in\ carry\ over\end{Bmatrix}$$

$$+\begin{Bmatrix}Char\ shrinking\ into\ the\\ interval\ from\ a\ larger\ size\end{Bmatrix}-\begin{Bmatrix}Char\ shrinking\ out\ of\ the\\ interval\ to\ a\ smaller\ size\end{Bmatrix}$$

$$-\begin{Bmatrix}Char\ depleted\ within\ the\\ interval\ due\ to\ combustion\end{Bmatrix}+\begin{Bmatrix}Ch\,ar\ generated\ within\ the\\ interval\ due\ to\ attrition\end{Bmatrix}=0 \tag{3.12}$$

Alternatively it takes the following form in symbols,

$$F_oP_o\left(r\right)\Delta r+F_{recy}P_{recy}\left(r\right)\Delta r-F_{bd}P_{bd}\Delta r-F_{co}P_{co}\Delta r+M_dP_{bed}\left(r\right)\left(-\frac{dr}{dt}\right)_{r+\Delta r}$$
$$-M_dP_{bed}\left(r\right)\left(-\frac{dr}{dt}\right)_r-\frac{3M_dP_{bed}\left(r\right)}{r}\left(-\frac{dr}{dt}\right)+U_f\left(r_f,0\right)F_aP_f\left(r\right)=0 \tag{3.13}$$

where F_a is the mass flow rate of attrition generated char particles the derivation of

which is given elsewhere [79]:

$$F_a = \int_{r_f}^{r_{max}} \frac{3M_d P_{bed}\left(r^*\right)}{r}\left(-\frac{dr^*}{dt}\right)_a \tag{3.14}$$

Dividing both sides of Equation (3.13) by Δr and taking $lim_{\Delta r \to 0}$ and rearranging the equation by using the assumptions (2), (3) and (4) Equation (3.13) becomes,

$$F_o P_o\left(r\right) + F_{recy} P_{co}\left(r\right) - F_{bd} P_{bd} - F_{co} P_{co} + \frac{d}{dr}\left[M_d P_{bed}\left(r\right)\Re\left(r\right)\right]$$
$$-\frac{3M_d P_{bed}\left(r\right)\Re\left(r\right)}{r} + U_f\left(r_f, 0\right) F_a P_f\left(r\right) = 0 \tag{3.15}$$

where $\Re(r)$ is the short notation for the shrinkage rate of char particles:

$$\Re\left(r\right) = -\frac{dr}{dt} \tag{3.16}$$

In order to express Equation (3.15) in more compact form, the unknowns, i.e., M_d, $P_{bed}(r)$, and $\Re(r)$ are combined in a dummy variable, which is defined as,

$$W\left(r\right) = M_d P_{bed}\left(r\right)\Re\left(r\right) \tag{3.17}$$

and inserted into the Equation (3.13) to yield the working form of the population balance as:

$$\frac{dW\left(r\right)}{dr} = -W\left(r\right)\left[\frac{F_{bd}}{M_d \Re\left(r\right)} + \left(1 - \frac{F_{recy}}{F_{elut}}\right)\frac{E\left(r\right)}{\Re\left(r\right)} - \frac{3}{r}\right] + F_o P_o\left(r\right) + U_f\left(r_f, 0\right) F_a P_f\left(r\right) \tag{3.18}$$

Equation (3.18) is subjected to the following boundary condition,

$$at\ r = r_{max} \qquad W(r) = 0 \tag{3.19}$$

as the probability of having solid particles of size r_{max} in the bed, *i.e.,* P_{bed}, is practically zero, due to the shrinkage of maximum particle size in the bed. Once the solution for $W(r)$ becomes available, the bed char hold-up, M_d, bed char size distribution, $P_{bed}(r)$, carryover rate, F_{co}, carryover char size distribution, $P_{co}(r)$, can be obtained by using the descriptions in Equations (3.9) and (3.17).

3.1.5 Desulfurization Model

It is generally accepted that desulfurization involves two consecutive steps, calcination of limestone followed by sulfation reaction. Endothermic decomposition of calcium carbonate ($CaCO_3$) to calcium oxide (CaO) and carbon dioxide (CO_2) is called calcination (see reaction 6 in Table 3.2). At low CO_2 partial pressures or/and high temperatures $CaCO_3$ calcines rapidly. However, at high CO_2 partial pressures or/and low temperatures calcination reaction is strongly disfavored. The percentage CO_2 at the outlet of a coal-fired ABFBC is typically 10-15 % and the temperature is about 850 °*C*. The equilibrium partial pressure of CO_2 at 850 °*C* is 0.48 bar, which means that the limestone remains uncalcined at pressures exceeding 4.8 bar for 10 % CO_2 in the stack gas, [80]. In addition, at atmospheric pressure it was found that the ultimate degree of calcination was maximum around 850 °*C*, which is very close to the temperatures utilized in this study. Therefore, in atmospheric pressure systems it is more convenient to assume that calcination of limestone particles is rapid, but slow enough to give homogeneous release of CO_2 in the emulsion phase.

Experiments performed by Scala *et al.* [81] to compare particle size distribution of the sorbent before and after calcination revealed that the decrease in

the mean diameter of the sorbent due to calcination was about 8 % and the increase associated with sulfation was 2 %, which means an overall decrease of 6 % in the sorbent mean diameter due to calcination and sulfation. Therefore, in this study it is assumed that particle size of sorbent does not change during reaction and the attrition of limestone particles are not considered. For the sake of clarity in notation, the formulations below are derived for a particular sorbent particle size and dependencies of the parameters on sorbent particle size is not shown explicitly.

Sulfation reaction occurs via the reaction 7 in Table 3.2. The sulfation kinetics are based on two simple assumptions: the sorbent sulfation rate, r_{SO_2}, is first order in the SO_2 concentration, C_{SO_2}, and first order in the external sorbent surface area, *S(t)* [45]:

$$r_{SO_2} = kC_{SO_2}S(t) \tag{3.20}$$

The former assumption was justified by Marsh and Ulrichson [82] in a detailed sulfation study. They showed that between 740 °*C* and 930 °*C*, the sulfation reaction is clearly first order in SO_2 concentration. Further, it was found that above 740 °*C*, sulfation reaction is zero order with respect to O_2 concentration in the case of excess O_2 in the gas phase.

The principle techniques for the determination of the reactivity of sorbents in ABFBC are the thermogravimetric analysis and fluidized bed combustion experiments. Although thermogravimetric analysis permits the study of gas-solid reactions in different conditions with respect to the reactant gas, this method is very poor in reproducing the real reaction conditions in ABFBC, first due to the fact that the limestone is subjected to calcination in CO_2 atmosphere before it is exposed to

sulfation in a simulated flue gas containing SO_2, and secondly it does not simulate the behavior of limestone in a dynamic environment, in which coal or other fuels are combusted in ABFBCs. In other words, by thermogravimetric analysis the reactivity of limestone, which only reflects sulfation characteristics of the limestone itself, is determined. Rather than reactivity of limestone, its sulfur capture capability in ABFBC conditions should be characterized. That is, parameters other than limestone reactivity such as fluidization and mixing conditions in the combustor, wide size distribution of limestone particles, effects of the interaction between fuel and sorbent in the combustor need to be taken into account. Consequently, a fluidized bed combustion test has to be carried out for the determination of sulfur capture performance of the limestone, which incorporates the effect of limestone reactivity and other operating parameters in real ABFBC conditions. This was also confirmed by Adanez *et al.* [83], who characterized the sulfur capture capability of eight different limestones by thermogravimetric analysis and fluidized bed combustion experiments. The comparisons showed the necessity of characterizing the limestone sulfur capture performance by fluidized bed combustion experiments. Sulfation rate constant, k, is used as a measure of sulfur capture capability of sorbent in the model developed in this thesis study. Therefore, in this study overall sulfation rate constant, which is a combination of film mass transfer limitations and sulfation kinetics, was determined from fluidized bed combustion experiment. Rather than using individual kinetic and mass transfer rate constants in the system model, overall sulfation rate constant was determined by using the sulfur retention efficiency determined experimentally, since overall sulfation rate constant slightly depends on the sorbent particle size (see Appendix B).

The conversion of freshly added sorbent in the combustor as a function of time can be obtained by the following equation,

$$\frac{dn_{CaO}}{dt} = -r_{SO_2} \tag{3.21}$$

which may be rearranged to obtain,

$$q_s \frac{dS(t)}{dt} = -kS(t)C_{SO_2} \tag{3.22}$$

where q_s is the surface CaO concentration and defined as,

$$q_s = \left[\frac{moles\ of\ CaO\ in\ a\ particle}{particle\ outer\ surface\ area} \right] \tag{3.23}$$

or in symbols,

$$q_s = \frac{1}{6M_{CaCO_3}} x_{CaCO_3} \rho_{lst} d_p \tag{3.24}$$

Fractional external surface area, $\sigma(t)$ is defined by dividing instantaneous surface area to initial surface area, S_0,

$$\sigma(t) = \frac{S(t)}{S_0} \tag{3.25}$$

where total initial external surface area for spherical limestone particles is expressed as:

$$S_0 = \frac{6M_{lst}}{\rho_s d_p} \tag{3.26}$$

Therefore, substituting Equation (3.25) into Equation (3.22) and rearranging:

$$\frac{d\sigma(t)}{dt} = -\frac{k}{q_s}\sigma(t)C_{SO_2} \tag{3.27}$$

Performing the integration, fractional external surface as a function of time is obtained:

$$\sigma(t) = exp\left[-\frac{kC_{SO_2}t}{q_s}\right] \tag{3.28}$$

In order to model sulfation reaction at steady state it is necessary to assess an average fractional external surface area, which can be calculated from the solids residence time distribution function, *E(t)*, and the fractional external surface area as a function of time according to,

$$\sigma_{avg} = \int_0^{\tau_{max}} E(t)\,\sigma(t)\,dt \tag{3.29}$$

where τ_{max} is the maximum possible reaction time and *E(t)* is defined as:

$$E(t) = \frac{1}{\tau}exp\left[-t/\tau\right] \tag{3.30}$$

By substituting the components and integrating Equation (3.27) an equation for average fractional external surface area is obtained:

$$\sigma_{avg} = \frac{1}{\left[1+\frac{kC_{SO_2}\tau}{q_s}\right]}\left[1-exp\left(-\left\{\frac{1}{\tau}+\frac{kC_{SO_2}}{q_s}\right\}\tau_{max}\right)\right] \tag{3.31}$$

Therefore rate of sulfation reaction rate becomes:

$$r_{SO_2} = kC_{SO_2}S_0\sigma_{avg} \tag{3.32}$$

Then the total reaction rate is the summation of the rates obtained at different sizes:

$$r_{SO_2} = \sum_{i=1}^{n} r_{SO_2,i} \tag{3.33}$$

Residence time of sorbent particles in the combustor is another important parameter for determination of extent of sulfation reaction. The sorbent particles with terminal velocities higher than the superficial gas velocity stay in the bed and the residence time of these particles in the bed section, τ_{bed} is conventionally defined as:

$$\tau_{bed} = \frac{limestone\ holdup\ in\ the\ bed}{limestone\ feed} \tag{3.34}$$

On the other hand, sorbent particles with terminal velocities smaller than the superficial gas velocity are carried to the freeboard by the gas and residence time of these particles, τ_{elut} is calculated by,

$$\tau_{elut} = \frac{H_f}{u_0 - u_t} \tag{3.35}$$

where u_t is the terminal velocity. Terminal velocities of the particles are calculated by using the correlation given by Kunii and Levenspiel [64]:

$$u_t = \begin{cases} \dfrac{g\left(\rho_p - \rho_g\right)d_p^2}{18\mu} & for\ Re_p \le 0.4 \\ \left[\dfrac{4}{225}\dfrac{\left(\rho_p - \rho_g\right)^2 g^2 d_p^3}{\rho_g \mu}\right]^{1/3} & for\ 0.4 < Re_p \le 500 \\ \left[\dfrac{3.1g\left(\rho_p - \rho_g\right)d_p}{\rho_g}\right]^{0.5} & for\ 500 < Re_p \le 200\ 000 \end{cases} \tag{3.36}$$

The residence time of recycled particles are calculated in the same way as the elutriated ones. However, it is difficult to determine the number of cycles of the recycled ash and sorbent particles through the combustion zone. An appropriate parameter to characterize the number of cycles, N_r, of the recycled sorbent and ash particles through the combustion zone, further explanation of which can be found in Appendix C, is defined by Vleeskens *et al.* [84]:

$$N_r = \frac{mass\ flow\ of\ recycled\ fly\ ash}{mass\ flow\ of\ discharged\ fly\ ash} \tag{3.37}$$

Therefore, if the residence time of a sorbent particle in the fly ash during one cycle through the combustion zone is τ_{elut} seconds, the mean residence time of that particle which is recycled N_r times is calculated from Equation (3.38):

$$\tau_{recy} = N_r \tau_{elut} \tag{3.38}$$

3.1.6 Mass and Energy Balance Equations

Spatial variations of species concentrations are described by the conservation equations for chemical species in bubble and emulsion phases:

$$\frac{dn_{j,b}}{dz} = A_{bed}\delta\left[\Re_{j,b} + K_{be}(C_{j,e} - C_{j,b})\right] \tag{3.39}$$

$$n_{j,e}\,|_{z=0} - n_{j,e} + V_{bed}\delta\left[\frac{1-\delta}{\delta}\varepsilon_{mf}\,\Re_{j,e} - K_{be}(C_{j,e} - \overline{C}_{j,b})\right] = 0 \tag{3.40}$$

These equations are subject to the following boundary conditions:

$$\text{at } z = 0 \qquad n_{j,b} = y_{j,b} \frac{n_a}{1 + \dfrac{u_e}{u_b} \dfrac{1-\delta}{\delta} \varepsilon_{mf}} \tag{3.41}$$

$$\text{at } z = 0 \qquad n_{j,e} = y_{j,e} \frac{n_a}{1 + \dfrac{u_b}{u_e} \dfrac{\delta}{(1-\delta)\varepsilon_{mf}}} \tag{3.42}$$

The expressions for the species generation or depletion terms appearing in Equations (3.39) and (3.40), $\Re_{j,b}$ and $\Re_{j,e}$, take the following forms for each species considered,

j=1 (O_2)

$$\Re_{1,b} = -0.5 r_{CO,b} \tag{3.43}$$

$$\begin{aligned} \Re_{1,e} = & -\frac{m_{vm} x_{vl}}{V_{bed}(1-\delta)\varepsilon_{mf}} \left\{ 0.5 \frac{x_{C,vm}}{M_C} + 0.5 \frac{x_{H,vm}}{M_{H_2}} + \frac{x_{S,vm}}{M_S} - \frac{x_{O,vm}}{M_{O_2}} \right\} \\ & - 0.5 n_{C,e} - 0.5 r_{CO,e} - \frac{0.5 r_{SO_2,e}}{V_{bed}(1-\delta)\varepsilon_{mf}} \end{aligned} \tag{3.44}$$

j=2 (CO)

$$\Re_{2,b} = -r_{CO,b} \tag{3.45}$$

$$\Re_{2,e} = \frac{m_{vm} x_{vl}}{V_{bed}(1-\delta)\varepsilon_{mf}} \left\{ 0.5 \frac{x_{C,vm}}{M_C} \right\} + n_{C,e} - r_{CO,e} \tag{3.46}$$

j=3 (CO_2)

$$\Re_{3,b} = r_{CO,b} \tag{3.47}$$

$$\Re_{3,e} = r_{CO,e} + \frac{F_{lst} x_{CaCO_3}}{M_{CaCO_3} V_{bed}(1-\delta)\varepsilon_{mf}} \tag{3.48}$$

j=4 (H_2O)

$$\Re_{4,b} = 0 \tag{3.49}$$

$$\Re_{4,e} = \frac{1}{V_{bed}(1-\delta)\varepsilon_{mf}} \left\{ m_{vm} x_{vl} \frac{x_{H,vm}}{M_{H_2}} + m_f \frac{x_{H_2O}}{M_{H_2O}} \right\} \tag{3.50}$$

j=5 (SO_2)

$$\Re_{5,b} = 0 \tag{3.51}$$

$$\Re_{5,e} = \frac{1}{V_{bed}(1-\delta)\varepsilon_{mf}} \left\{ \frac{m_{vm} x_{vl} x_{S,vm}}{M_S} - r_{SO_2,e} \right\} \tag{3.52}$$

where,

$$n_{C,e} = \frac{3W_d}{V_{bed}(1-\delta)\varepsilon_{mf}} \int_{r_{\min}}^{r_{\max}} \frac{P_{bed}(r)}{r} \Re(r) dr \tag{3.53}$$

On the assumption that the gas and the inert particles are at the same temperature and that the mass of combustion gases and char particles are negligible compared to the mass of inerts, a combined gas/solid phase energy balance can be written as,

$$\begin{aligned} &\frac{1}{c_{pi} M_i} \left\{ n_A \int_{T_r}^{T_A} c_{pA} dT - \alpha \frac{A_T}{L_T} \int_0^{L_T} U_{cw}(T_{bed} - T_{cw}) dx - A_{bw} h_{bw}(T_{bed} - T_{bw,s}) \right. \\ &- m_{recy} c_{pi} \left(T_{bed} - T_{recy}\right) - m_{co} c_{pi}(T_{bed} - T_r) - m_{bd} c_{pi}(T_{bed} - T_r) \\ &\left. - n_g \sum_{j=1}^{6} y_j \int_{T_r}^{T_{bed}} c_{pg,j} dT - m_f x_w \lambda^0 + Q_{rxn} + Q_p \right\} = 0 \end{aligned} \tag{3.54}$$

where enthalpy generated by chemical reactions, Q_{rxn}, and energy transferred from burning char particles, Q_p, are obtained from following equations,

$$Q_{rxn} = m_f x_{vm} x_{vl} \left[\frac{x_{C,vm}}{M_C} \Delta H^0_{R2} + \frac{x_{H,vm}}{M_{H_2}} \Delta H^0_{R4} + \frac{x_{S,vm}}{M_S} \Delta H^0_{R5} \right] - \frac{F_{lst} x_{CaCO_3}}{M_{CaCO_3}} \Delta H^0_{R6}$$
$$+ A_{bed} \left\{ \Delta H^0_{R3} \left[\varepsilon_{mf}(1-\delta) \int_0^{H_{bed}} r_{CO,e} dz + \delta \int_0^{H_{bed}} r_{CO,b} dz \right] + \frac{\Delta H^0_{R7}}{V_{bed} \varepsilon_{mf}(1-\delta)} \int_0^{H_{bed}} r_{SO_2,e} dz \right\} \quad (3.55)$$

$$Q_p = \frac{3M_d}{\rho_d} \int_{r_{min}}^{r_{max}} \left[h_p(T_d - T_{bed}) + \sigma\varepsilon(T_d^4 - T_{bed}^4) \right] \frac{dr}{r} \quad (3.56)$$

and particle temperature is calculated by solving an energy balance around the particle, which is assumed to have uniform temperature:

$$\frac{\rho_d}{M_C} \frac{x_{fc}}{x_{fc} + x_a} \Delta H^o_{R1} \Re(r) - \left[h_p \left(T_d - T_{bed} \right) + \sigma\varepsilon \left(T_d^4 - T_{bed}^4 \right) \right] = 0 \quad (3.57)$$

Energy loss through the bed walls is taken into account by making a one-dimensional heat transfer analysis. For a combustor with square cross-section and wall thickness of L_{bw}, the temperature profile inside the wall of variable cross section is given by the following equation:

$$\frac{d^2 T_{bw}}{dx^2} \left(x + A_{bed}^{0.5} / 2 \right) + \frac{dT_{bw}}{dx} = 0 \quad (3.58)$$

Equation (3.58) is subject to the following boundary conditions:

$$\begin{aligned} &at\ x = 0 \qquad h_{bw} \left(T_{bed} - T_{bw} \right) = -k_{bw} \frac{\partial T_{bw}}{\partial x} \\ &at\ x = L_{bw} \qquad T_{bw} = T_{bw,o} \end{aligned} \quad (3.59)$$

In order to account for the energy absorbed by the in-bed heat exchanger, a separate

energy balance is performed on the cooling water. Neglecting the heat transfer resistance of the tubes, the spatial variation of the temperature of the cooling water is given by the following equation:

$$\frac{4m_{cw}}{\pi}\frac{dT_{cw}}{dx}-\frac{4d_{T,o}}{c_{pcw}}h_{cw}\left(T_{bed}-T_{w}\right)=0 \tag{3.60}$$

The inlet temperature of the cooling water is set as boundary condition to Equation (3.60). Surface temperature of tube wall, T_w, is calculated by solving a surface energy balance:

$$h_{cw}d_{T,o}\left(T_{bed}-T_{w}\right)-h_{i}d_{T,i}\left(T_{w}-T_{cw}\right)=0 \tag{3.61}$$

3.2 Freeboard Model

3.2.1 Solids distribution

The hold-up of particles in the freeboard is expressed with an exponential decay function Choi et al. [63],

$$\frac{\varepsilon_{s}}{\varepsilon_{s,0}}=\exp\left(-az_{f}\right) \tag{3.62}$$

where $\varepsilon_{s,0}$ is the volume fraction of solids just above the surface of dense bubbling bed and is given by:

$$\varepsilon_{s,0}=1-\varepsilon_{f} \tag{3.63}$$

The volume fractions of char and inert particles of size *r* at bed surface are obtained from the following equations, respectively:

$$\varepsilon_{d,0} = \varepsilon_{s,0} \frac{W_d P_{bed}(r)\Delta r / \rho_d}{W_d / \rho_d + W_i / \rho_i} \tag{3.64}$$

$$\varepsilon_{i,0} = \varepsilon_{s,0} \frac{W_i P_{bed}(r)\Delta r / \rho_i}{W_d / \rho_d + W_i / \rho_i} \tag{3.65}$$

The entrainment flux of particles, K_i^*, is calculated by assuming that it consists of a cluster flux, K_{ih}^*, and a dispersed noncluster flux, $K_{i\infty}^*$ as suggested by Hazlett and Bergougnou [85],

$$K_i^* = K_{ih}^* + K_{i\infty}^* \tag{3.66}$$

and are obtained from empirical correlations proposed by Choi *et al.* [63]. The elutriation rate constant, *E(r)*, defined in Equation (3.7) is then calculated from:

$$E(r) = \frac{A_{bed}}{W_d} K_{i\infty}^* \tag{3.67}$$

The elutriated particles are assumed to rise at the superficial gas velocity in the freeboard. Size distribution of entrained solid particles at any height in the freeboard is calculated by assuming that probability of finding particles of size *r* at any height is proportional to their presence in bed with proportionality constant being K_{ih}^*:

$$F_z P_z(r) = K_{ih}^* A_{bed} P_{bed}(r) \tag{3.68}$$

Multiplying both sides of Equation (3.67) by *dr* and integrating yields the flow rate of entrained particles and their size distribution as follows:

$$F_z = A_{bed} \int_{r_{\min}}^{r_{\max}} K_{ih}^{*} P_{bed}(r) dr \tag{3.69}$$

$$P_z(r) = A_{bed} K_{ih}^{*} P_{bed}(r) / F_z \tag{3.70}$$

3.2.2 Mass and Energy Balance Equations

It is assumed that the gases in the bubble and emulsion phases mix instantaneously at the top of the bed and enter freeboard. The gas flow in freeboard is assumed to be in plug flow. A shell mass balance for j^{th} gas component in the freeboard results in the following equation:

$$\frac{dn_{j,f}}{dz} = A_f (1-\varepsilon_s) \Re_{j,f} \tag{3.71}$$

Boundary condition for Equation (3.71) is expressed as:

$$at\ z_f = 0 \qquad n_{j,f} = n_{j,e} + n_{j,b} \tag{3.72}$$

The expression for species generation/depletion term, $\Re_{j,f}$, appearing in Equation (3.71)takes the following forms for the species considered,

j=1 (O_2)

$$\Re_{1,f} = -\frac{m_{vm}(1-x_{vl})}{V_f(1-\varepsilon_s)} \left\{ 0.5\frac{x_{C,vm}}{M_C} + 0.5\frac{x_{H,vm}}{M_{H_2}} + \frac{x_{S,vm}}{M_S} - \frac{x_{O,vm}}{M_{O_2}} \right\} - \frac{0.5 r_{SO_2,f}}{V_f(1-\varepsilon_s)} - 0.5 n_{C,f} - 0.5 r_{CO,f} \tag{3.73}$$

j=2 (CO)

$$\Re_{2,f} = \frac{m_{vm}(1-x_{vl})}{V_f(1-\varepsilon_s)}\left\{0.5\frac{x_{C,vm}}{M_C}\right\} + n_{C,f} - r_{CO,f} \tag{3.74}$$

j=3 (CO_2)

$$\Re_{3,f} = r_{CO,f} \tag{3.75}$$

j=4 (H_2O)

$$\Re_{4,f} = \frac{m_{vm}(1-x_{vl})}{V_f(1-\varepsilon_s)}\left\{\frac{x_{H,vm}}{M_{H_2}}\right\} \tag{3.76}$$

j=5 (SO_2)

$$\Re_{5,f} = \frac{1}{V_f(1-\varepsilon_s)}\left\{m_{vm}(1-x_{vl})\frac{x_{S,vm}}{M_S} - r_{SO_2,f}\right\} \tag{3.77}$$

where $n_{C,f}$, the solid carbon consumption rate at any height in freeboard is the sum of carbon consumption rates for coarse and fine particles, as shown below,

$$n_{C,f} = -\frac{2\eta}{M_C}\frac{x_{fc}}{x_{fc}+x_a}\left[\rho_d \int_{r_{\max e}}^{r_{\max}} \frac{\varepsilon_{s,d}P_z(r)}{r}\Re_f(r)dr + \frac{F_{co}}{A_f}\int_{r_{\min}}^{r_{\max}} \frac{P_{co}(r)}{r\,u_p(r)}\Re_f(r)dr\right] \tag{3.78}$$

η in Equation (3.78) represents the contact efficiency between gas and solids in freeboard and it is calculated from the following equation proposed by Kunii and Levenspiel [86],

$$\eta = 1-(1-\eta_0)\exp(-6.62\,z_f) \tag{3.79}$$

where,

$$\eta_0 = \frac{u_e}{u_0}(1-\delta) \tag{3.80}$$

The gas temperature profile in freeboard is obtained by solving an energy balance which considers convective transport and, generation and loss of energy:

$$\frac{dT_f}{dz} = \frac{A_f(1-\varepsilon_s)}{n_f c_{p,g}} \boldsymbol{R} \tag{3.81}$$

Equation (3.81) has the following boundary condition:

$$at\ z = 0 \qquad T_f = T_{bed} \tag{3.82}$$

$\boldsymbol{R}$ is the combined energy generation and loss rate per unit volume of freeboard. It is the sum of energy generated by chemical reactions, $\boldsymbol{R_{rxn}}$, energy loss from freeboard walls, $\boldsymbol{R_{fw}}$, and energy transferred from/to char and ash particles present in the freeboard, $\boldsymbol{R_p}$. These terms can be expressed as follows:

$$\boldsymbol{R_{rxn}} = \Delta H^0_{R3} r_{CO,f} + \frac{m_{vm}(1-x_{vl})}{V_f(1-\varepsilon_s)}\left[\frac{x_{C,vm}}{M_C}\Delta H^0_{R2} + \frac{x_{H,vm}}{M_{H_2}}\Delta H^0_{R4} + \frac{x_{S,vm}}{M_S}\Delta H^0_{R5}\right] + \frac{r_{SO_2,f}}{V_f(1-\varepsilon_s)}\Delta H^0_{R7} \tag{3.83}$$

$$\boldsymbol{R_{fw}} = -\frac{4d_{bed}}{A_{bed}(1-\varepsilon_s)} h_{fw}(T_f - T_{fw}) \tag{3.84}$$

$$\begin{aligned}\boldsymbol{R_p} = {} & \frac{3F_{co}}{A_{bed}\rho_d}\int_{r_{\min}}^{r_{\max e}} \frac{P_{z,d}(r)}{r\,u_p(r)}\left[h_p(T_d - T_f) + \sigma\varepsilon(T_d^4 - T_f^4)\right]dr \\ & + 3\varepsilon_d \int_{r_{\max e}}^{r_{\max}} \frac{P_{z,d}(r)}{r}\left[h_p(T_d - T_f) + \sigma\varepsilon(T_d^4 - T_f^4)\right]dr \\ & + 3\varepsilon_i \int_{r_{\max e}}^{r_{\max}} \frac{P_{z,i}(r)}{r}\left[h_p(T_i - T_f) + \sigma\varepsilon(T_i^4 - T_f^4)\right]dr\end{aligned} \tag{3.85}$$

It is assumed that in freeboard char particles temperatures are equal to their temperatures in bed as calculated by Equation (3.57) and temperatures of inert particles remain at T_{bed}. A surface energy balance is formulated to solve for the temperature of the freeboard wall,

$$h_f\left(T_f - T_{fw}\right) - \frac{\left(T_{fw} - T_{fw,o}\right)}{R_w} = 0 \tag{3.86}$$

where h_f is calculated by using the approach of Kunii and Levenspiel [64]:

$$\frac{h_f - \left(h_r + h_g\right)}{h_{zf=0} - \left(h_r + h_g\right)} = \exp\left(-a\, z_f / 2\right) \tag{3.87}$$

3.3 Solution Procedure

The input data required by the system model are the configuration of the rig and its internals, air and coal flow rates, coal analysis, all solid and gas properties, inlet temperatures of air, cooling water and feed solids and the size distribution function of feed solids deduced from sieve analysis.

Apart from these input data, application of the model necessitates empirical and semi-empirical correlations from the literature for heat and mass transfer, combustion kinetics, elutriation and entrainment rates *etc.*, listed in Tables 3.1 and 3.2. These expressions contain empirical or semi-empirical constants which may not always comply with the experimental conditions of the system to be modeled. Therefore, it is the usual practice to adjust some of these constants until a compromise is found to reproduce the measured data as accurately as possible [76]. In this study, minimum number of fitting parameters was utilized. These were pre-exponential factor for carbon monoxide oxidation, exponential decay constant for

entrained particles and elutriation rate constant.

CO concentrations predicted by using the rate expression of Hottel *et al*. [72] was found an order of magnitude lower than the measurements. To match the measured *CO* concentration at the exit of the combustor, the rate constant from Hottel et al. was multiplied by 0.3 and this value was used for model validation.

With regard to entrainment, direct use of the entrainment rate expression of Choi *et al.* [63], in the model resulted in higher char hold-up and hence lower O_2 concentrations in the freeboard compared to measurements. To match the measured O_2 concentration at the exit of the freeboard, the decay constant of the entrainment rate expression of Choi *et al.* was multiplied by 5 and used in the simulations for model validation.

Direct use of elutriation rate expression of Choi *et al.* [63] in the model yielded higher carryover flow rate at the cyclone exit. To match the measured carryover flow rates, elutriation rate constant of Choi *et al*. was multiplied by 0.06 for Run 1 and 0.09 for Runs 2 and 3. Fine-tuning for the carryover flow rates at the cyclone exit was the simplest approach as the carryover flow rate was only a function of elutriation.

The solution starts with making initial guesses for T_{bed}, $\bar{y}_{O_2,e}$, M_d, F_a, $T_{bw,o}$. This is followed by computation of $\overline{T}_d$ by using estimated parameters. There are five loops of iterations to be converged for T_{bed}, $\bar{y}_{O_2,e}$, M_d, F_a, $\overline{T}_d$. For each loop, a convergence criterion, ε, is set as the absolute difference between calculated and estimated values of the parameters. Figure 3.3 shows the algorithm of the steady state model code in compact form.

The predictions reported in this study were obtained with ε values of 5×10^{-3}, 5×10^{-5}, 5×10^{-5}, 5×10^{-2} and 5×10^{-1} for iterations on M_d, F_a, $\bar{y}_{O_2,e}$, $\overline{T}_d$, T_{bed}, respectively. The integration of ODEs is carried out by Backward-Differentiation Formula (BDF) method embedded in the ODE solver LSODES [87]. Solution of the non-linear algebraic equations is performed by using the subroutine ZERO. Details of the solution procedure of steady state code can be found in [60].

The total CPU time for the complete model is about 290 seconds on 400 MHz Intel Pentium II computer.

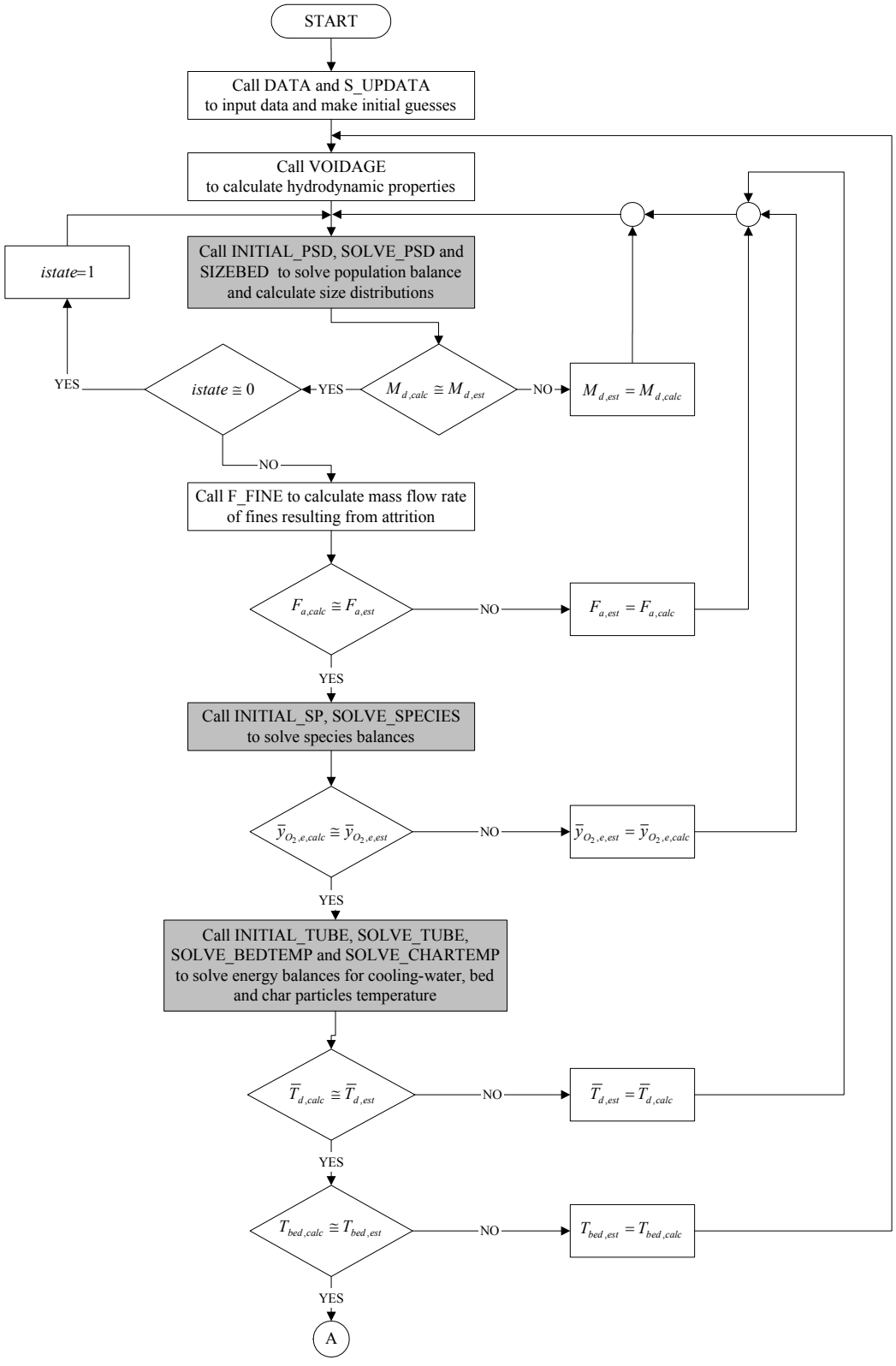

Figure 3.3 Algorithm for the steady state code showing the modified sections in this study in shade.

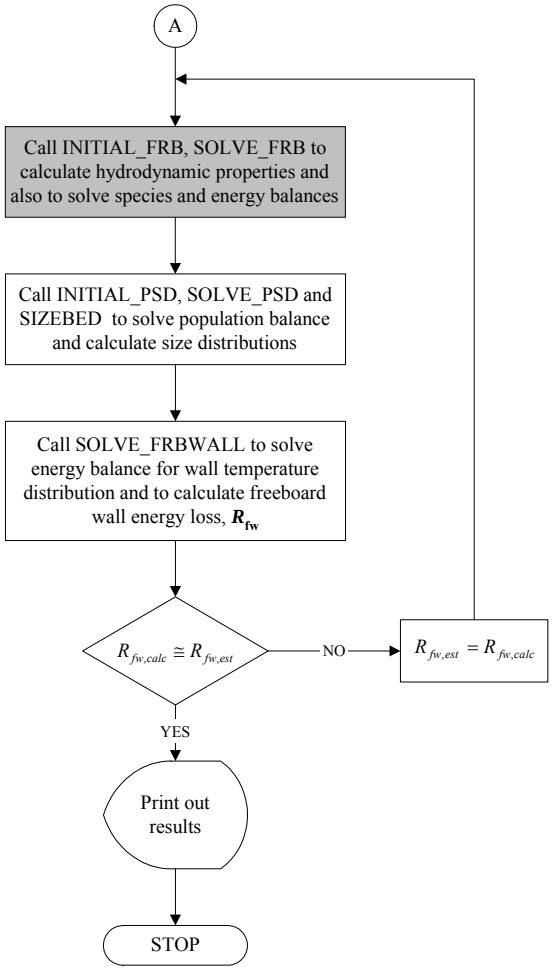

Figure 3.3 Algorithm for the steady state code showing the modified sections in this study in shade (continued).

CHAPTER 4

EXPERIMENTAL SET-UP AND CONDITIONS

4.1 0.3 MW_t ABFBC Test Rig

Experimental work was carried out on a 0.3 MW_t ABFBC Test Rig designed and constructed within the scope of a cooperation agreement between Middle East Technical University (METU), Babcock & Wilcox GAMA (BWG) under the auspices of Canadian Development Agency (CIDA) for the investigation of combustion and in-situ desulfurization characteristics of low quality Turkish lignites. The existing test rig was extended to incorporate a baghouse filter for capture of fine fly ash leaving with the flue gas through the stack within the scope of a recent research project, MİSAG-159, financed by The Scientific and Technical Research Council of Turkey (TÜBİTAK). The test rig in its present form is shown schematically in Figure 4.1. As can be seen from the figure, the test rig basically consists of a forced draft (FD) fan, a windbox with an ash removal system, a

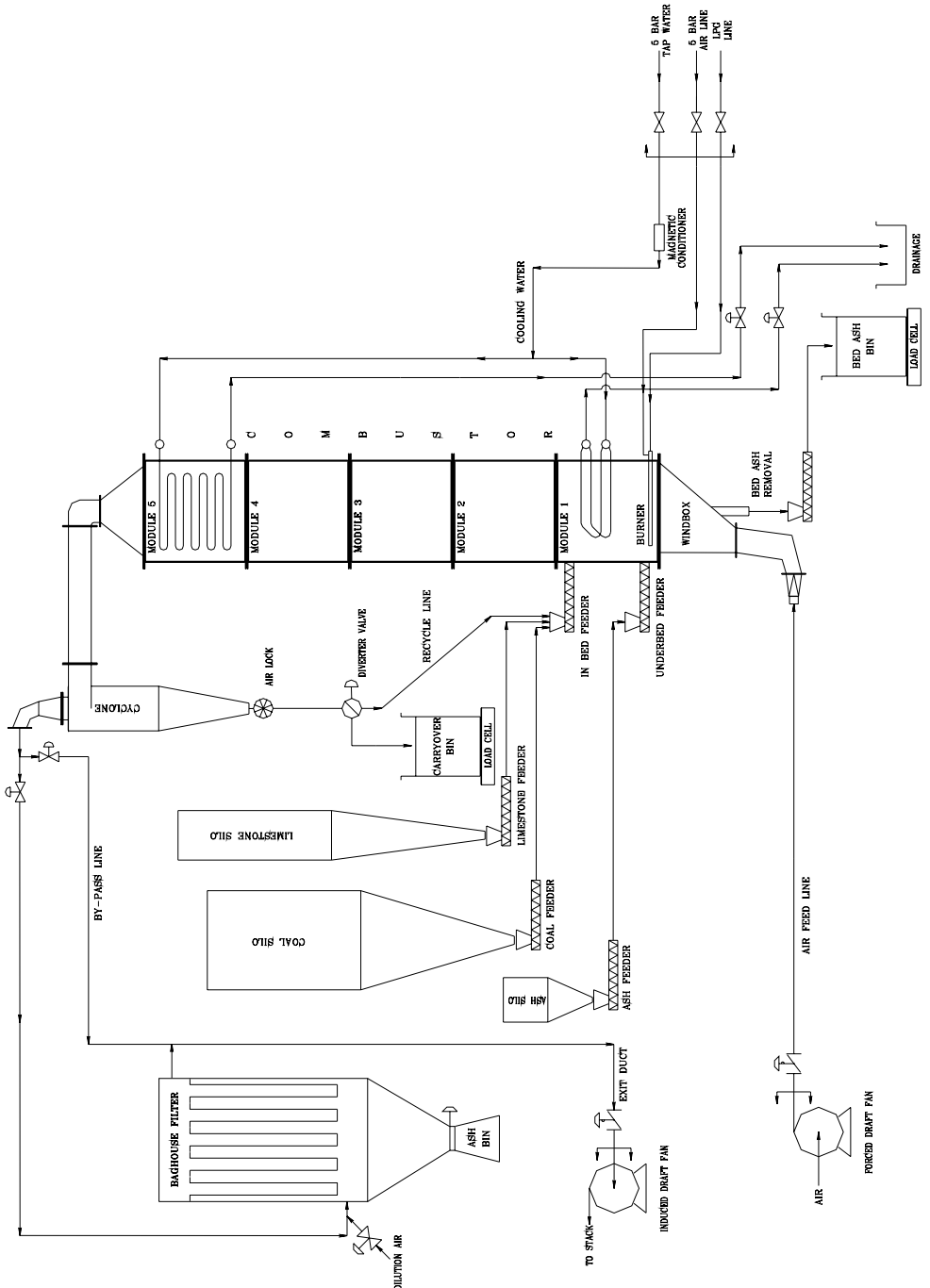

Figure 4.1 Flowsheet of 0.3 MW_t ABFBC Test Rig.

modular combustor, a cyclone with a recycle leg, a baghouse filter, an induced draft (ID) fan and a coal and limestone feeding system.

4.1.1 The Combustor

The main body of the test rig is the modular combustor formed by five modules of equal dimensions. Modular structure of the combustor is intended to provide flexibility in burning various fuels by addition or removal of heating surfaces. Each module has an internal cross-section of $0.45 \times 0.45\ m^2$ and 1 *m* height. Inner walls of each module are refractory lined with firebricks with a thickness of 6 *cm*. Outer walls of the refractory bricks are insulated with insulation bricks with thickness of 20 *cm*. Further insulation is provided by leaving an air gap of 6 *mm* between the outer wall of insulation brick and the inner wall of the steel construction of each module.

The first and fifth modules from the bottom are referred as bed and cooler, respectively, and the ones in between are referred as freeboard modules. The bed module provides an expanded bed height of 1 *m*. It contains 6 water-cooled U-tubes (25 *mm* OD, stainless steel) for cooling purposes, 5 ports for thermocouples, 4 ports for gas sampling probes, one port for LPG distributor, one port for the ignitor and two ports for feeding coal/limestone mixture. One of the feeding ports is 22 *cm* and the other is 85 *cm* above the distributor plate. There are 6 ports for gas sampling probes and 9 ports for thermocouples in freeboard and cooler modules. There exists a water-cooled tube bundle consisting of 11 tubes (26.7 *mm* OD, carbon steel) with 14 passes installed across the cross-section of the cooler module for cooling the stack gases before leaving the combustor.

4.1.2 Air and Gas System

The fluidizing air fed by the FD fan enters the bottom of the windbox through a pipe of 6.5 *m* long and 7.8 *cm* ID on which a manual gate valve, an automatic butterfly valve and a vortex flowmeter are installed. The design of the windbox allows the installation of bed ash removal system as shown in Figure 4.1. It is a mobile windbox supported by four wheels and a distributor plate is placed on the top. Air supplied to the windbox by means of the pipe of 7.8 *cm* ID diverges to the full cross-section of the combustor at the distributor plate located 1.4 *m* above the entrance port. Sieve type distributor plate contains 412 holes, each 4.5 *mm* in diameter, arranged in a triangular pattern. Within the bed module air mixes with lignite and limestone to affect combustion and sulfur capture.

Flue gases and elutriated fines leaving the bed surface enter the freeboard. Sufficient freeboard height is provided to permit burnout of elutriated lignite fines and combustible gases.

After leaving the freeboard, flue gases pass through the cooler module to cool the hot combustion gases. Flue gases leaving the modular combustor enter the cyclone and then the baghouse filter to leave the elutriated particles before passing through ID fan to exit from the stack. As the temperature of the flue gases entering the baghouse filter is limited by the maximum operating temperature of the bag material which is 260 *°C* for the bag material (P84-Polyimide) selected for the baghouse filter under consideration, two alternative systems were provided for the safe operation of the baghouse filter: A bypass line between the cyclone and the ID fan and an air dilution system to reduce the flue gas temperature at the inlet to the filter through a slide valve if the temperature exceeds the upper operating limit of the bag material.

The pipes carrying the flue gases before and after the baghouse filter are 14.0 and 5.3 *m* long, respectively, and have an ID of 15.3 *cm*. The pipeline between the cyclone and the ID fan of the existing test rig before the incorporation of baghouse filter was used as the bypass line. It has an ID of 12.8 *cm* and length of 14.5 *m*. The outlet of the baghouse filter joins this pipeline 4.2 *m* before the ID fan.

An orifice meter with a bore diameter of 8.05 *cm* was installed at the stack gas line before ID fan to measure the flow rate of the flue gases. The pressure drop across the orificemeter is measured by means of pressure transmitter. Knowing the temperature and pressure of the flue gases passing through the orificemeter, the signal from the transmitter is interpreted in the control system to yield molar flow rate.

4.1.3 Solids Handling System

Crushed and sieved lignite and limestone are stored in two separate silos and conveyed into the hoppers of feeders at controlled flow rates via precalibrated volumetric feeders placed under their respective silos. The lignite/limestone mixture is continuously fed to the bed through water-cooled screw feeders. Both screw feeders are operated at controlled speed in such a way as to maintain certain amount of accumulated material in the hopper in order to prevent backflow of combustion gases from the combustor.

Bed ash is withdrawn from the bed through 5 *cm* diameter, 1.1 *m* long water-cooled ash removal pipe. Some of the bed ash is disposed and the rest is stored to provide bed inventory when required. Bed ash drain rate is adjusted from the computer to obtain the desired bed pressure drop and hence the expanded bed height. Bed ash particles are collected in a continuously weighted ash storage bin.

The majority of the elutriable fines produced from solid in the bed and those fed within the solid streams are captured by the cyclone, having dimensions of 45 *cm* OD and 2.12 *m* height. Cyclone catch particles pass through an air lock (i.e. a rotary valve) and fall onto a diverter. Depending on the position of the diverter, particles are either discharged from the system to a continuously weighted ash storage bin for experiments without recycle or flow back to the combustor for refiring. The fraction of a short time interval over which the position of the diverter remains on the recycle mode determines the recycle ratio. Continuity of flow is provided by repeating this time interval periodically. In order to provide a wider range of recycle ratio and yet not to disturb the steady state conditions within the combustor, a periodic time interval of 10 *s* was selected.

In order to catch fine particles of fly ash ($d_p \leq 40\ \mu m$) leaving the cyclone, a *pulse-jet* type baghouse filter with a 100 *%* collection efficiency for particles greater than 1 μm was utilized. As mentioned in the previous section, the bag material used is P84-Polyimide and it can resist temperatures up to 260 °*C*. Hence, if the inlet temperature of the flue gases exceeds 220 °*C* dilution or bypass of flue gases is employed.

Before putting the baghouse filter into service, a permanent *pre-coat* is formed on the outer surface of the bags in order to increase the collection efficiency solely provided by the porosity of the bag material itself. This is accomplished by passing the fine *CaO* particles through the filter. During the service, an additional filter cake is built up at the outer surface of the bags which in turn becomes a principal collection medium. As the filter cake gets thicker with time, a pulse of compressed air is directed into the bag from the open top, which causes a shock wave to travel down its length dislodging the filter cake from the outer surface of

the bag. A unique aspect of the pulse jet system is the use of a wire cage in each bag to keep it from collapsing during normal filtration. The bag hangs from the tube sheet. A series of parallel pulse jet pipes are located above the bags with each pipe row having a solenoid valve. This allows the bags to be pulsed clean one row of five bags at a time. Filter cake cleaned off the surface fall into a hopper and is discharged to fly ash collecting container. There are two containers each having a volume of 0.13 m^3. During filtration of flue gases if one container gets full, the maximum level device gives alarm by lighting the level warning light located on control panel, and the container full of ash is replaced with the other one after closing the ash discharge opening by leak proof slide valve.

4.1.4 Cooling Water System

Cooling water required for the test rig is passed through a magnetic conditioner and is then divided into two streams, one for the in-bed tube bundles, the other for the tube bundle in the cooler module. Heat transfer areas provided by the bed and cooler modules are 0.30 m^2 and 4.3 m^2, respectively. The cooling water in bed enters lower header and leaves the bed through the upper header. The cooling water for the cooler module enters the upper header and flows downward to provide counter-current flow to the up flowing flue gases. Water flow rates are adjusted by means of either a manual or a pneumatic control valve located at the drain of each stream to maintain maximum exit temperature of about 60 $°C$.

4.1.5 Gas Sampling System

Benefits of using advanced analytical instrumentation are negated unless a representative sample from the point of extraction can be obtained. Areas of

concern in continuous gas sampling pointed out in detail by Anthony *et al*. [88] can be summarized as follows:

1. A sample must be subjected to minimum thermal chemical or fluid-mechanical disturbances by the sampling system. It is necessary to quench gas phase reactions at the point of sampling particularly when analyzing for minor constituents such as NO_x and CO.
2. The sample must be conditioned and transported to the analyzers without changing the concentration ratios of components to be measured. Conditioning is essential as the analyzers are designed to operate at near ambient temperatures and pressures and with dry, particulate free, non-corrosive, non-interfering samples. Therefore, particular care must be taken in gas sample cleanup to remove the particulates that are characteristic of Atmospheric Fluidized Bed Combustors (AFBC) and to remove the excess moisture that might otherwise condense in the sampling lines or analyzer banks.

   Another problem is that gaseous species may be partly lost along the transport line because of homogeneous or catalytic reactions or simply by absorption of gas phase species such as SO_2 in the condensate is another possible source of error, while subsequent desorption can lead to erroneously high values when sampling lower concentrations.
3. In order to accurately measure the species of interest the analyzers must also be properly calibrated and maintained.
4. The sample extraction system must be durable because of the high-temperature, corrosive atmosphere present in the combustor.

Once through the probe, the sampled combustion gas is passed through a solenoid valve and sent to the gas conditioning and analysis system of the test rig by means

of sample line. The sample line itself is maintained at 150 °C by means of a variable DC power supply so that no water, sulfuric acid or hydrocarbons would condense along the sampling interface. In addition, all lines and fittings in contact with the gas sample are made of teflon or stainless steel to prevent interferences due to gas adsorption or heterogeneous reactions. The existing analytical system of the test rig consists of a bank of analyzers for O_2, CO, CO_2, SO_2 and NO/NO_x. The positions of the gas sampling probes and the details of gas conditioning and analysis system are given in Table 4.1 and Figure 4.2, respectively. Gas is sampled at a rate of 13 cm^3/s at STP which is small enough to cause minimal interference to the combustion system. After passing through the probe, sample gas is transported through the heated stainless steel line to a hygroscopic, ion exchange membrane type gas drier. Once through the drier, the gas is cooled, filtered and pumped to the analyzers via a teflon-coated diaphragm-type sample pump. Then, sample gas is divided into two

Table 4.1 Relative positions of gas sampling probes.

Probe No	**Distance above the distributor plate, *cm***
P10	26
P9	56
P8	69
P7	85
P6	123
P5	183
P4	291
P3	344
P2	419
P1	500

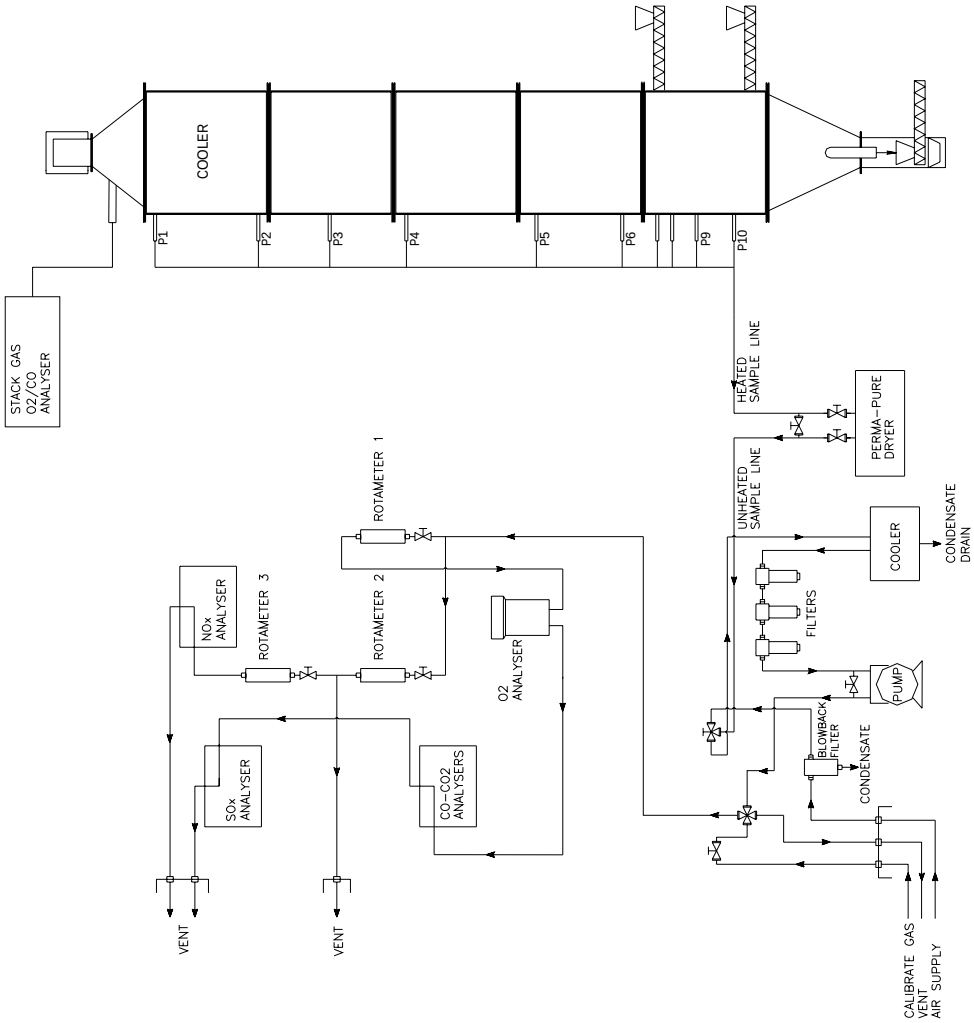

Figure 4.2 Gas conditioning and analysis system.

parallel lines; one passing through O_2, CO/CO_2 and SO_2 analyzers in series, the other through NO/NO_x analyzer. After the measurement of species concentrations, sample gas is vented to the atmosphere. On-line wet analyses of O_2 and CO are also carried out at the exit of the combustor.

4.2 Instrumentation and Analytical Systems

Instrumentation and analytical systems can be divided into following categories:

- Data acquisition and control system
- Solid flow control and monitoring
- Air and gas flow control and monitoring
- Cooling-water flow control and monitoring
- On-line continuous gas analyzers
- Pressure sensors
- Temperature sensors
- Solids analyses

The test rig is equipped with a data acquisition and control system namely Bailey INFI 90. Real time process data is monitored, manipulated, collected and analyzed with the aid of a control software called Bailey LAN-90 Process Control View installed on an IBM compatible PC 486 computer running under QNX operating system. The control system scans the signals coming from all of the instruments attached to it in a fraction of a second and reports and logs their averages discretely for 30 seconds of intervals. An uninterruptible power supply is connected to Bailey INFI 90 and PC in order to enable proper shut-down in case of a electricity cut-off by preventing corruption of data logged.

Fuel and sorbent feed rates are controlled manually by adjusting the fuel feeder or sorbent feeder control dial from the computer. The flow rates of fuel and sorbent are normally set to such values that provide desired excess air and *Ca/S* molar ratio, respectively. Bed ash drain rate can also be adjusted from the computer to obtain the desired bed pressure drop and hence the expanded bed height. The interface between the controller and driving motors of fuel and sorbent feeders and bed ash drain are provided with three speed transmitters. Cyclone ash and bed ash are collected in respective bins and their flow rates are followed by load cells placed under respective bins.

The volumetric flow rate of air is measured by a vortex flow meter and adjusted with an automatic butterfly valve driven by a computer controlled pneumatic actuator. In order to achieve conversion from volumetric to molar flow, a static pressure tap and a temperature sensor is placed downstream of the vortex flow meter. The flow rate of air is normally set to a value to achieve the desired superficial velocity in the combustor. In order to achieve almost neutral pressure on the bed surface, the flow rate of exhaust gases is adjusted with an automatic butterfly valve driven by a computer controlled pneumatic actuator.

In order to measure flow rates of cooling-water flowing through bed and cooler bundles, two orifices are located up streams of their lower and upper headers, respectively. The pressure drops across the orificemeters are measured by means of pressure transmitters. The signals from the transmitters are interpreted in the control system to yield mass flow rate of the cooling-water flowing through in-bed and cooler bundles. There exist two pneumatic control valves installed on the downstream of upper and lower headers of bed and cooler bundles, respectively, to adjust the cooling-water flow in each bundle. The flow rates of cooling-water in bed

and cooler bundles are normally set to a value which provide exit water temperature in the range 40-60 °*C*.

The on-line continuous gas analyzers with which the test rig is equipped are listed in Table 4.3. Analyzers except Bailey SMA 90 are used for measuring spatial variation of species O_2, CO, CO_2, NO/NO_x and SO_2 along the combustor at the positions given in Table 4.2 on dry basis. Bailey SMA 90 uses close-coupled sampling system which does not remove water vapor from the sample. The analyzer reports CO equivalent indicating mostly CO, but also responds to other combustibles present in the flue gas. It is used for measuring temporal variation of O_2 and CO at the combustor exit.

Table 4.2 On-line gas analyzers.

Instrument	Gas species	Sensor type	Range
Leeds & Northrup	O_2	Paramagnetic	0-15 %
Anarad AR 600	CO	IR	0-5 %
	CO_2	IR	0-20 %
Siemens Ultramat 6	SO_2	NDIR	0-1 %
Servomex 1491	NO/NOx	Chemiluminescence	0-0.2 %
Bailey SMA 90	O_2	Zirconium oxide	0-25 %
	CO	Catalytic RTD	0-2 %

Pressure sensors are used for measuring differential and gauge pressures at various positions on the test rig. Measured differential pressures are the pressure drops over orificemeters, bed and distributor plate pressure drop, and gauge pressures are the pressure at the bed surface and pressure of air feed at the downstream of the vortex flow meter.

Spatial and temporal variations of gas temperatures along the height of the combustor are measured by means of thermocouples of K type (Chromel-Alumel) with grounded junction to minimize their response time. The tips of the thermocouples are on the symmetry axis of the combustor. The axial positions of thermocouples are given in Table 4.3. The temperature of air feed at the downstream of vortex flow meter and temperatures of cooling water at the exits of bed and cooler bundles are measured by resistance thermocouples of type Pt-100. Further details of the test rig and operating procedures such as procedures before cold start-up, during runs, after shut down can be found elsewhere [89].

Table 4.3 Relative positions of thermocouples.

Thermocouple No	**Distance above the distributor plate, *cm***
TC1	25
TC2	44
TC3	73
TC4	73
TC5	97
TC6	133
TC7	154
TC8	226
TC9	257
TC10	285
TC11	330
TC12	361
TC13	425
TC14	500

4.3 Experimental Conditions

4.3.1 Coal and Sorbent Characteristics

Experiments were carried out with Beypazarı lignite. Beypazarı lignite supplied by Turkish Coal Enterprises (TKİ) was delivered from Çayırhan lignite mine to Çayırhan Power Station of Turkish Electricity Generation and Transmission Co. (TEAŞ) where the coal to be burned in the test rig was prepared by crushing and sieving it through –4/+1.5 mm screens twice. Crushed and sieved lignite was then transported to the laboratory in closed barrels. Representative samples from coals were then subjected to sieve analyses and proximate and ultimate analyses. The results of these analyses together with the calorific values and particle densities determined by mercury porosimetry are summarized in Table 4.5. As can be seen from the table, Beypazari lignite is a fuel with high VM/FC ratio (~2), high ash content (~42 %) and high total sulfur content (~4.7 %). Ash constituents of lignite is

Table 4.5 Characteristics of Beypazarı lignite.

Sieve Analysis		**Proximate Analysis (as received)**		**Ultimate Analysis (dry)**	
Size (*mm*)	**Weight (%)**	**Component**	**Weight (%)**	**Component**	**Weight (%)**
4.000-3.350	13.6	Moisture	14.3	C	37.2
3.350-2.360	18.5	Ash	35.2	H	2.9
2.360-2.000	15.3	VM	31.5	O	14.9
2.000-1.700	13.8	FC	19.0	N	1.3
1.700-1.180	12.0	HHV: 3030 *cal/g*		S_{comb}	2.9
1.180-0.710	13.8	d_{32}: 0.86 *mm*		S_{total}	4.8
0.710-0.000	12.0	ρ_p: 1.58 g/cm^3		Ash	41.1

shown in Table 4.5. Very low calcium content of Beypazarı lignite ash is uncommon to the same lignite investigated previously [13].

Table 4.5 Ash analyses of the lignite.

Component	**Weight (%)**
SiO_2	45.0
Al_2O_3	15.9
Fe_2O_3	7.7
CaO	1.0
MgO	3.0
SO_3	16.2
Na_2O	8.0
K_2O	1.5
TiO_2	1.8

Limestone utilized in the firing tests was supplied by Park Thermic, Electric Industry and Trade, Inc. and originates from Acıbaşı limestone quarry, 10 *km* away from the Çayırhan Thermal Power Plant. Limestone delivered to the laboratory had a particle size below 6 *cm*. It was subjected to size reduction by crushing it in a jaw-crusher and a hammer mill consecutively. Crushed limestone was sieved through a 1.18 *mm* sieve and top product was crushed again by hammer mill. Particles under the sieve were utilized in the experiments. A representative sample from limestone was subjected to sieve and chemical analyses and the results are summarized in Table 4.6.

Table 4.6 Characteristics of Beypazarı limestone.

Size Distribution		**Chemical Analysis (dry)**	
Size (*mm*)	**Weight (*%*)**	**Component**	**Weight (*%*)**
1.180-1.000	11.2	$CaCO_3$	94.7
1.000-0.850	14.5	$MgCO_3$	0.7
0.850-0.710	5.8	SiO_2	4.8
0.710-0.600	6.0	Na_2O	0.1
0.600-0.500	6.5	K_2O	0.1
0.500-0.425	9.3	Al_2O_3	0.7
0.425-0.300	13.8	Fe_2O_3	0.5
0.300-0.250	19.8	LOI	40.8
0.250-0.150	6.9	d_{32} : 0.32 *mm*	
0.150-0.000	6.2	ρ_p: 2.40 g/cm^3	

4.3.2 Operating Conditions

In all the runs, the lignite was burned in its own ash due to its high ash content. Moreover, it was necessary to burn this lignite with a sorbent addition due to its high combustible sulfur content. In order to investigate the sulfation characteristics of the lignite under consideration experiments with limestone addition were carried out at two different recycle rates. Table 4.7 lists the operating conditions for all experiments. Experiments consists of 3 runs at Ca/S molar ratios of 3.0, 3.1 and 4.0 for Runs 1, 2 and 3, respectively. Run 1 was performed without recycle whereas Runs 2 and 3 were carried out at a recycle ratio of 0.86 and 0.84, respectively. Feed point location was 0.85 *m* above the distributor plate for all experiments. The experiments reported in this thesis study as Runs 1, 2 and 3 refer to the experiments coded as 021214.

Table 4.7 Operating conditions of the experiments.

	Run 1	**Run 2**	**Run 3**
Coal flow rate, *kg/h*	102	102	102
Limestone flow rate, *kg/h*	25	26	33
Ca/S molar ratio	3.0	3.1	4.0
Bed drain flow rate, *kg/h*	13	14	12
Cyclone ash flow rate, *kg/h*	34	38	37
Baghouse filter ash flow rate, *kg/h*	1.0	2.1	6.2
Recycle ratio*	0.0	0.86	0.84
Air flow rate, *kmol/h*	19	19	19
Excess air, *%*	30	29	29
Superficial velocity, *m/s*	2.5	2.5	2.4
Average bed temperature, *°C*	853	830	820
Average freeboard temperature, *°C*	839	854	824
Bed height, *m*	0.67	0.67	0.67
Feed point location, *m*	0.85	0.85	0.85
OHTC in the bed, W/m^2-*°C*	255	271	268
OHTC in the freeboard, W/m^2-*°C*	36	40	40
Bed cooling water flowrate, *kg/h*	1772	1784	1806
Freeboard cooling water flowrate, *kg/h*	2307	4774	4829

* Recycle ratio = (Recycle flow rate)/(Coal flow rate)

CHAPTER 5

RESULTS AND DISCUSSION

The assessment of the accuracy of the present system model in conjunction with sulfur retention model developed in this study was carried out by predicting the behavior of the lignite-fired 0.3 MW ABFBC test rig for the lignite characteristics and operating conditions shown in Tables 4.5, 4.8 and comparing the predictions with measurements. Axial temperature profiles, concentration profiles of O_2, CO, CO_2 and SO_2 throughout the combustor, gaseous emissions and sulfur retention efficiencies were used as measures of performance to test the validity of the model.

The input data required by the model includes the following:

- Configuration and dimensions of the test rig and its internals.
- Air and coal flow rates.
- Coal and limestone analyses.
- All solid and gas properties.
- Size distribution function of feed solids deduced from sieve analysis.

- Inlet temperatures of air, cooling water, and feed solids.

The following sections describe the comparison between measured and predicted temperature and concentration profiles, sulfur retention efficiencies and a model sensitivity analysis on the parameters related to sulfur capture.

5.1 Temperature Profiles

Figures 5.1-5.3 show the predicted and measured temperature profiles for the Runs 1-3, respectively. Inspection of the temperature profiles for all runs shows that temperature along the bed and freeboard remains almost constant. The fall in gas temperature toward the exit is due to the presence of the cooler in the final module. Predicted and measured values are found to be in good agreement in all runs.

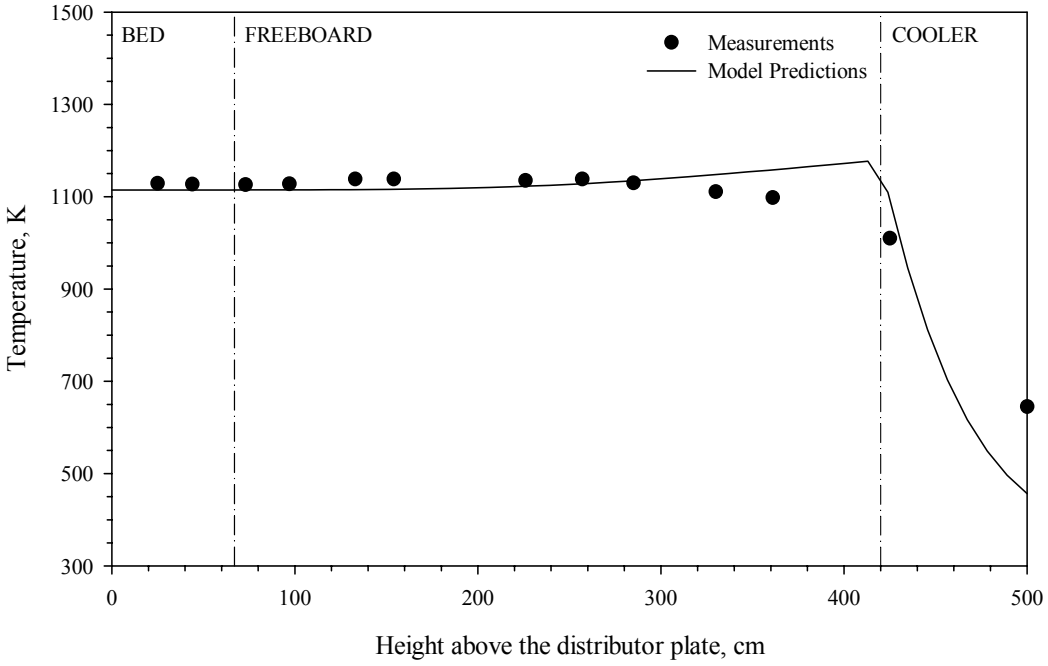

Figure 5.1 Measured and predicted temperature profiles for Run 1.

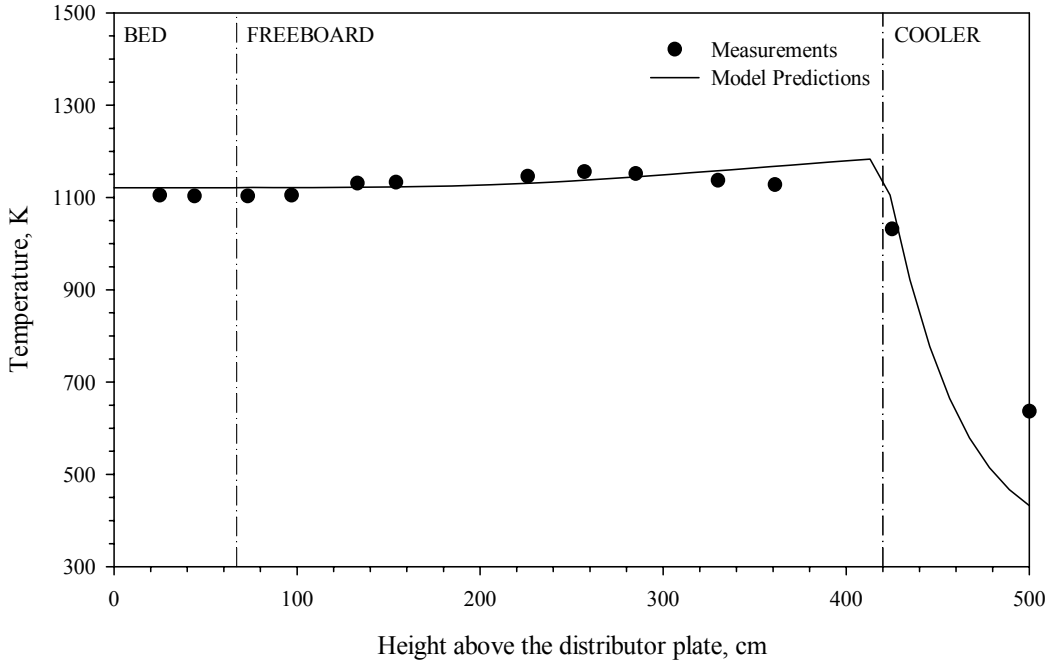

Figure 5.2 Measured and predicted temperature profiles for Run 2.

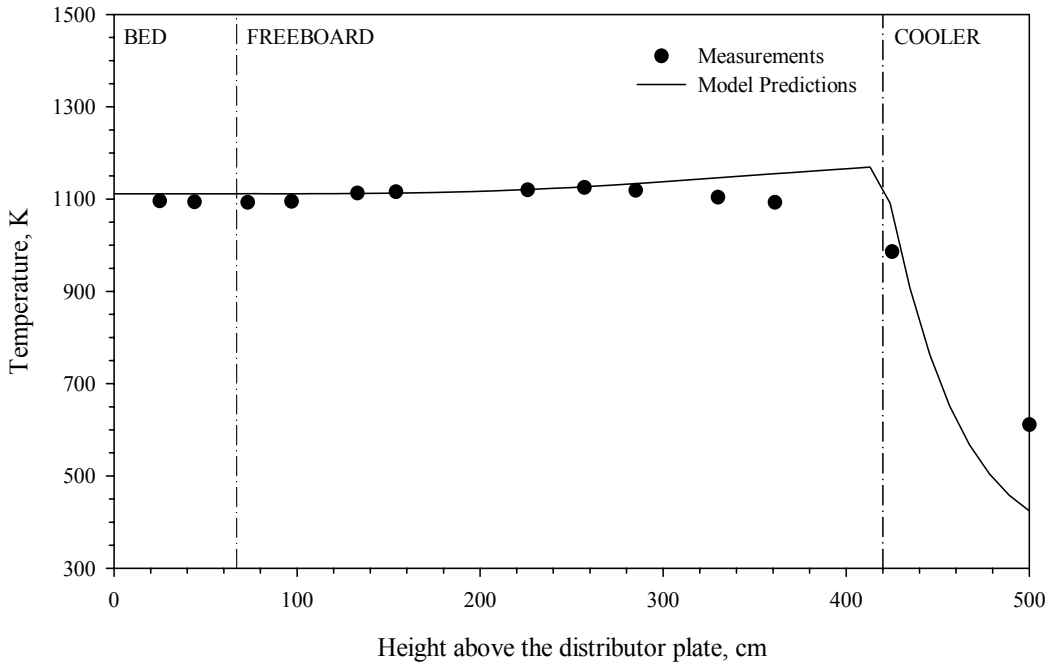

Figure 5.3 Measured and predicted temperature profiles for Run 3.

5.2 O_2, CO_2 and CO Concentration Profiles

Figures 5.4-5.6 compare the predicted and measured concentrations of O_2, CO_2 and CO along the combustor for Runs 1, 2, and 3, respectively. As can be seen from the figures, measured O_2 concentrations decreases until the bed surface whereas the measured CO_2 concentrations display an opposite trend in the same region. As for the freeboard section, the decrease in O_2 and increase in CO_2 concentrations keep on but with a lower slope. CO measurements, on the other hand, show maxima in the bed and decrease gradually along the freeboard with a lower slope. These profiles indicate that majority of the combustibles are burned in the bed section but not insignificant combustion also taking place in freeboard. As depicted in the Figures 5.4-5.6, favorable comparisons are also obtained between the predicted and measured profiles

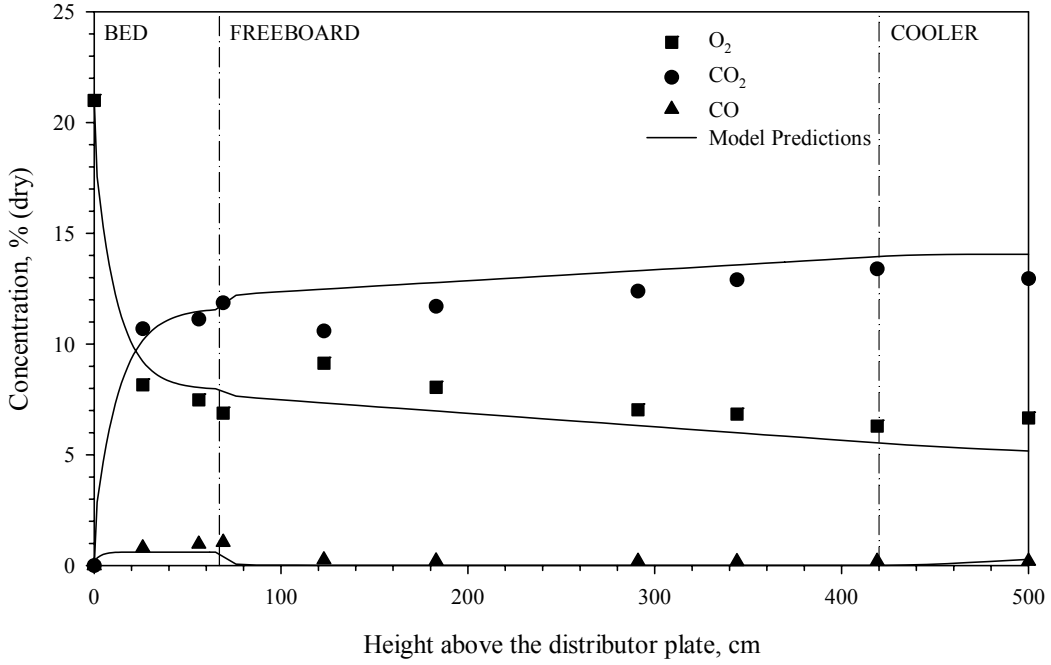

Figure 5.4 Measured and predicted O_2, CO_2, and CO concentrations for Run 1.

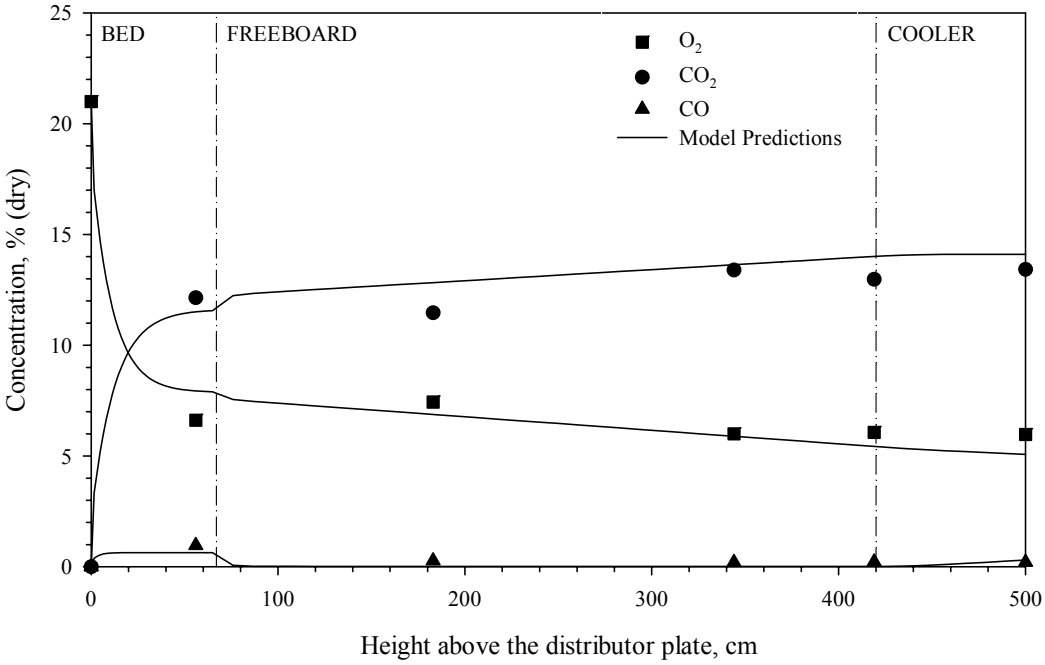

Figure 5.5 Measured and predicted O_2, CO_2, and CO concentrations Run 2.

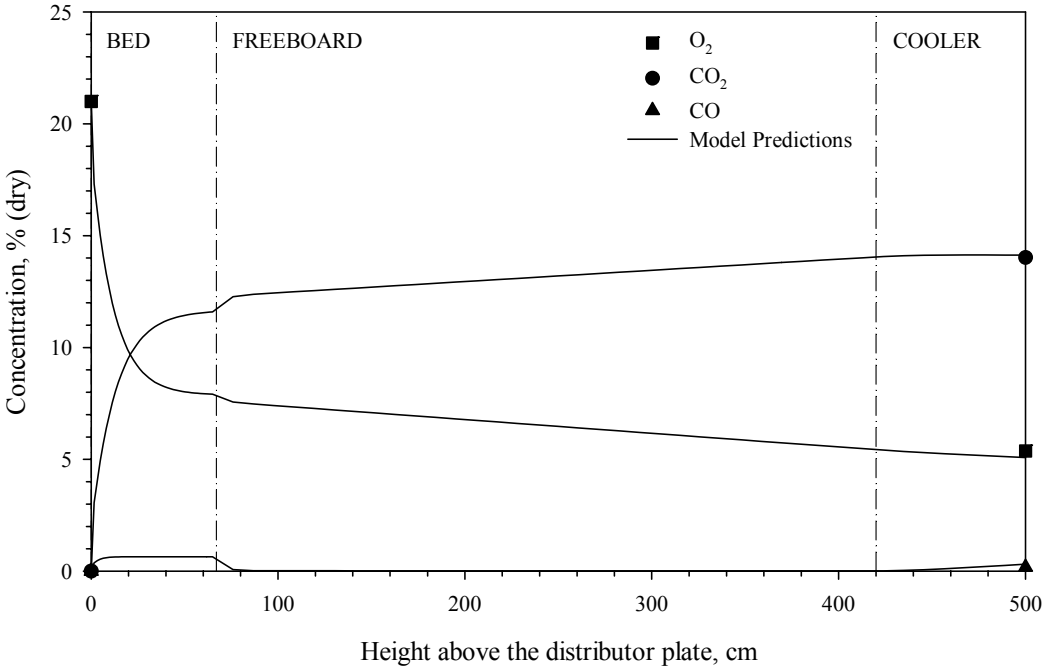

Figure 5.6 Measured and predicted O_2, CO_2, and CO concentrations Run 3.

Measured gaseous emissions together with model predictions are presented in Table 5.1. As displayed in this table, good agreement between experimental emissions and model predictions of the respective species is a consequence of the agreement between measured and predicted profile of these species.

Table 5.1 Gaseous emissions of the runs on dry basis.

	O_2, %		CO_2, %		CO, %		SO_2, *ppm*	
	Model	**Exp.**	**Model**	**Exp.**	**Model**	**Exp.**	**Model**	**Exp.**
Run 1	5.2	6.7	14.1	13.0	0.3	0.2	1368	1369
Run 2	5.1	6.0	14.1	13.4	0.3	0.2	680	872
Run 3	5.1	5.4	14.1	14.0	0.3	0.2	499	283

5.3 SO_2 Concentration Profiles

Steady state SO_2 concentrations measured along the combustor within the scope of these thesis were plotted in Figure 5.7 together with those measured previously in the experiments without limestone addition [58] to demonstrate the release and capture behavior of SO_2. Experiments without limestone addition consist of 3 runs carried out at recycle ratios of 0.0, 0.56 and 2.37 for Runs 1, 2 and 3, respectively. Both sets of experiments, with and without limestone addition, were carried out by using the same lignite under similar operating conditions. Comparisons reveal that SO_2 emissions of the experiments without limestone addition (≈4000 *ppm*) are over and above the limits imposed by the national air quality control regulations. Hence, the high sulfur containing lignite under consideration has to be burned with limestone addition.

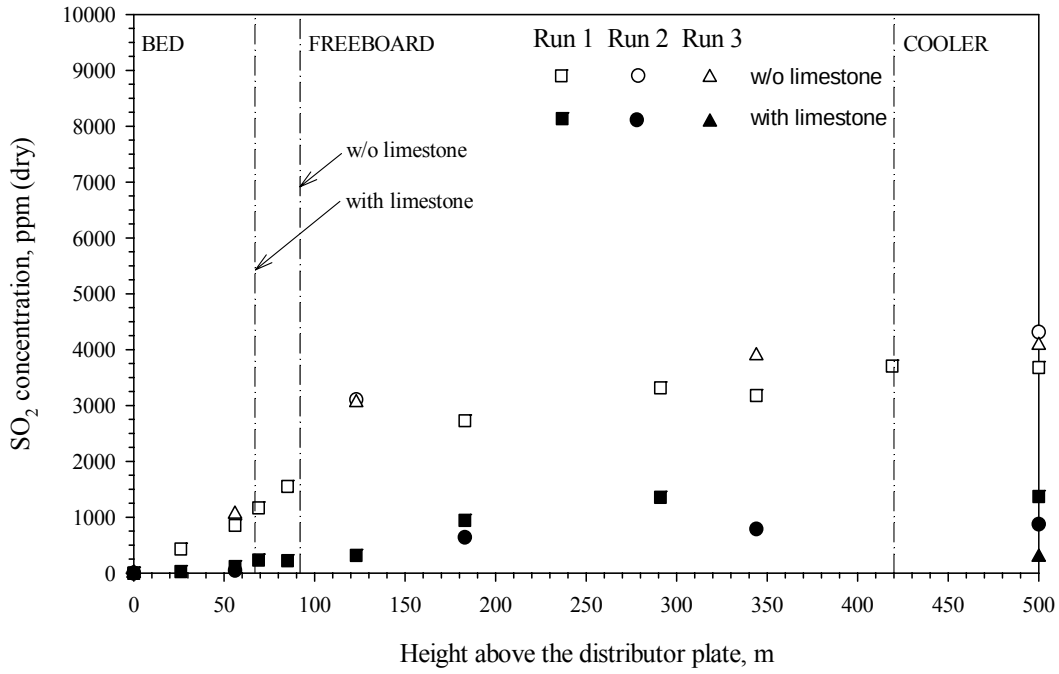

Figure 5.7 Measured SO_2 concentrations for the experiments with and w/o limestone.

As can be seen from Figure 5.7, SO_2 concentration increases continuously and levels off toward the exit. Higher, SO_2 concentrations in the freeboard compared to those in the bed are noteworthy. This is considered to be due to progressive release of volatiles throughout the combustor, which implies the necessity of sulfur capture up in the freeboard.

As depicted in Figure 5.7, SO_2 concentration is not affected by the recycle rate in the experiments without limestone addition, since the lignite contains negligible amount of inherent calcium.

Comparison between SO_2 concentrations near bed surface in experiments without sorbent addition (about 2000 *ppm*) and those with sorbent addition (about 200-250 *ppm*) indicates that SO_2 capture mainly takes place in the bed section

where the residence time of the sorbent particles is higher than that in the freeboard.

The effect of recycle on SO_2 concentrations for the experiments with limestone addition can be observed by comparing measurements of Run 1 and 2, both having the same *Ca/S* ratio. SO_2 concentration is found to decrease with recycle as expected. Increasing *Ca/S* ratio from 3.1 (Run 2) to 4.0 (Run 3) results in even lower SO_2 concentrations at the same recycle ratio. This can also be observed more quantitatively from the SO_2 emissions given in Table 5.1.

Sulfation rate constant obtained by using the experimental sulfur retention efficiency of Run 1 was found to be 14.9 *cm/s*. This value is very close to the values reported in the literature [55, 76]. The same sulfation rate constant was used as input data for the system model for simulation of the other two runs. Steady state SO_2 concentrations measured and predicted by the model are shown in Figures 5.8-5.10. Predicted SO_2 concentration profiles are in reasonable agreement with the experimental data in the freeboard region for all runs. However, there is a small discrepancy between measured and predicted SO_2 concentrations in the bed section. This may be considered to be due to the biasing of the compositions of the samples taken from the bed towards the composition of the slowest moving gas (emulsion phase), where SO_2 concentration is lower.

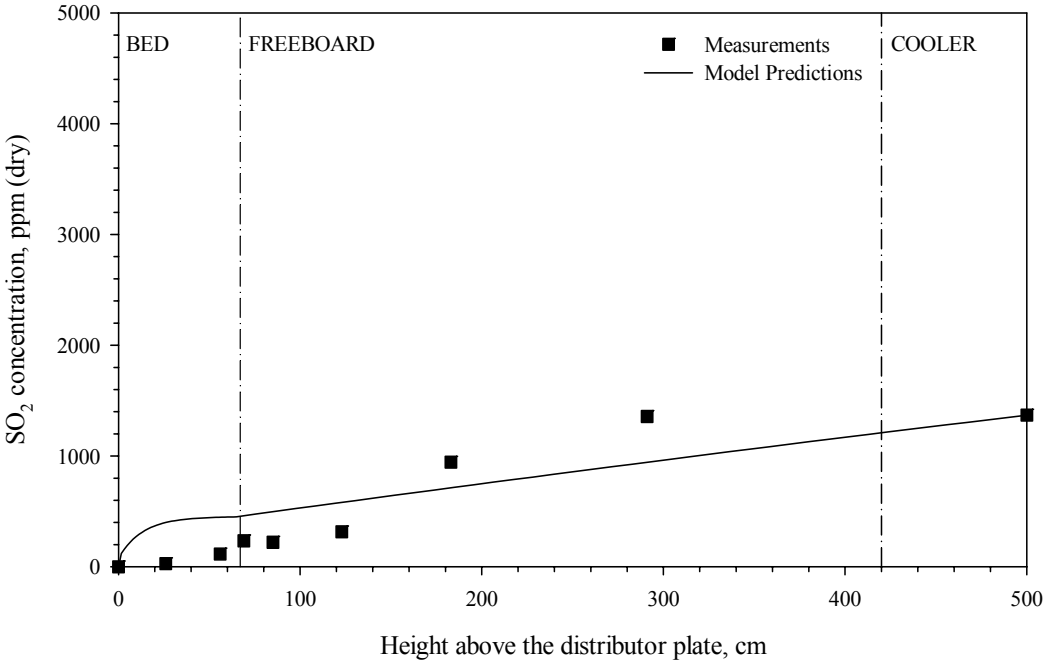

Figure 5.8 Measured and predicted SO_2 concentrations for Run 1.

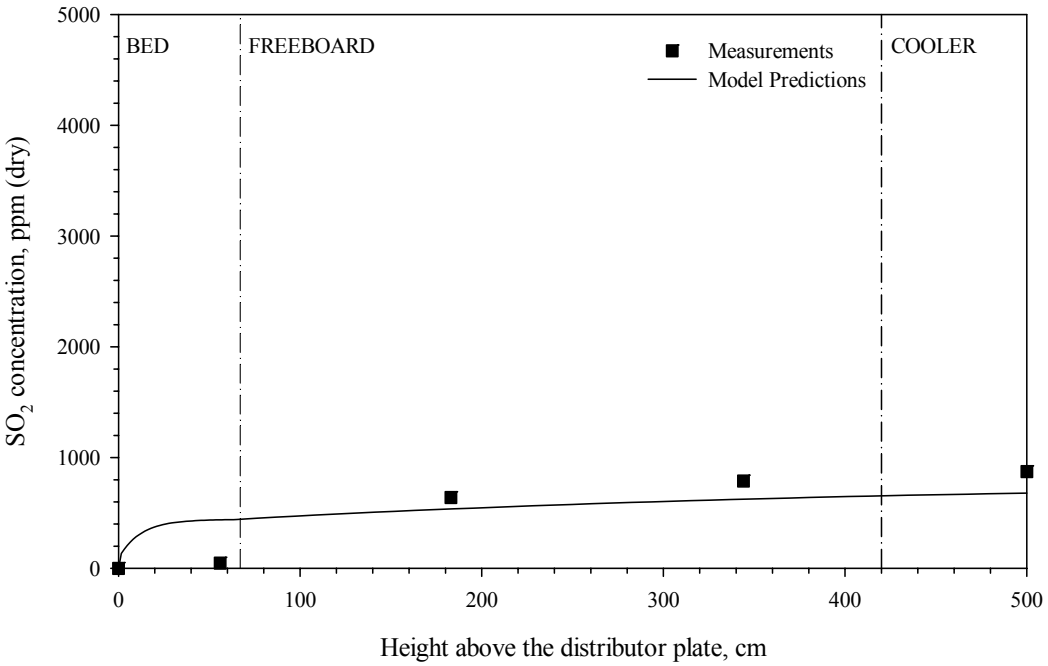

Figure 5.9 Measured and predicted SO_2 concentrations for Run 2.

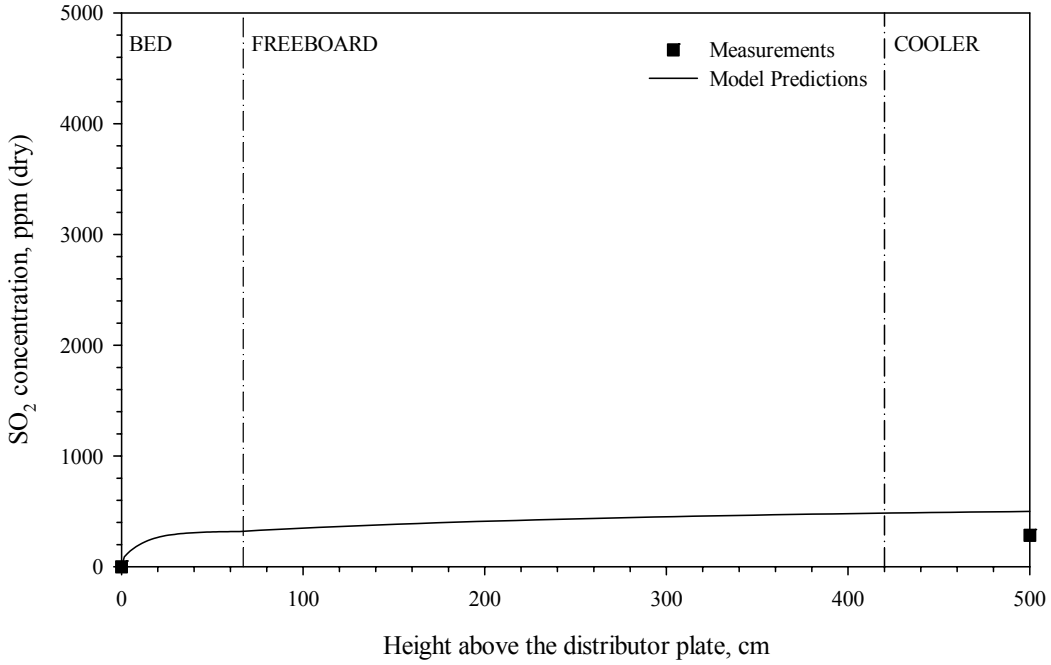

Figure 5.10 Measured and predicted SO_2 concentrations for Run 3.

5.4 Sulfur Retention Efficiencies

Table 5.2 lists the sulfur retention efficiencies obtained for all runs. Introduction of recycle in Run 2 increases the sulfur retention efficiency from 68.5 to 81.1 *%* due to the enhancement of calcium utilization from 23 to 26 *%* as a consequence of the increased residence time of unreacted or partially sulfated fine limestone particles recycled. Higher *Ca/S* ratio utilized in Run 3 results in an increase in sulfur retention efficiency from 81.1 to 93.6 *%* but with lower calcium utilization. Sulfur retention efficiencies and calcium utilizations predicted by the model are also presented in Table 5.2. Comparisons reveal that, model predicts sulfur retention efficiency and calcium utilization reasonably well.

Table 5.2 Sulfur retention efficiencies and *Ca* utilizations of runs with limestone.

	Ca/S	**Sulfur retention efficiency,** *%*		***Ca* utilization,** *%*	
		Model	Exp.	Model	Exp
Run 1	3.0	67.8	68.5	23	23
Run 2	3.1	84.0	81.1	27	26
Run 3	4.0	88.3	93.6	22	23

Sulfur capture in the bed and freeboard sections as predicted by the model is shown in Table 5.3 for all runs. In the run without recycle (Run 1) total sulfur retention efficiency of 67.8 *%* is predicted by the model, 3.5 *%* of which takes place in the freeboard section while 64.3 *%* sulfur capture takes place in the bed section. This may be considered to be due to the insufficient residence time of sorbent particles in the freeboard section. Therefore, it may be concluded that majority of the sulfur capture takes place in the bed section in operations without recycle. However, with the introduction of recycle (Run 2) the freeboard sulfur capture increases up to 19.5 *%*, leading to higher sulfur retention efficiency at the same *Ca/S* ratio.

Table 5.3 Sulfur captured in the bed and in the freeboard as predicted by the model.

	Sulfur Retention Efficiency, *%*		
	Bed	**Freeboard**	**Total**
Run 1	64.3	3.5	67.8
Run 2	64.5	19.5	84.0
Run 3	67.5	20.8	88.3

5.5 Model Sensitivity Analysis

Several parametric studies were performed in order to test the sensitivity of the model against operating parameters such as *Ca/S* ratio and recycle ratio. Figure 5.11 shows the effect of *Ca/S* ratio on the SO_2 concentration profile for the operations without recycle. Inspection of the figure shows that, at lower *Ca/S* ratios (< 1.5), effect of an increase in *Ca/S* ratio on the SO_2 concentration profile is significant whereas at higher *Ca/S* ratios (> 3.0) this effect is not pronounced. This is a consequence of lower calcium utilization at higher *Ca/S* ratios.

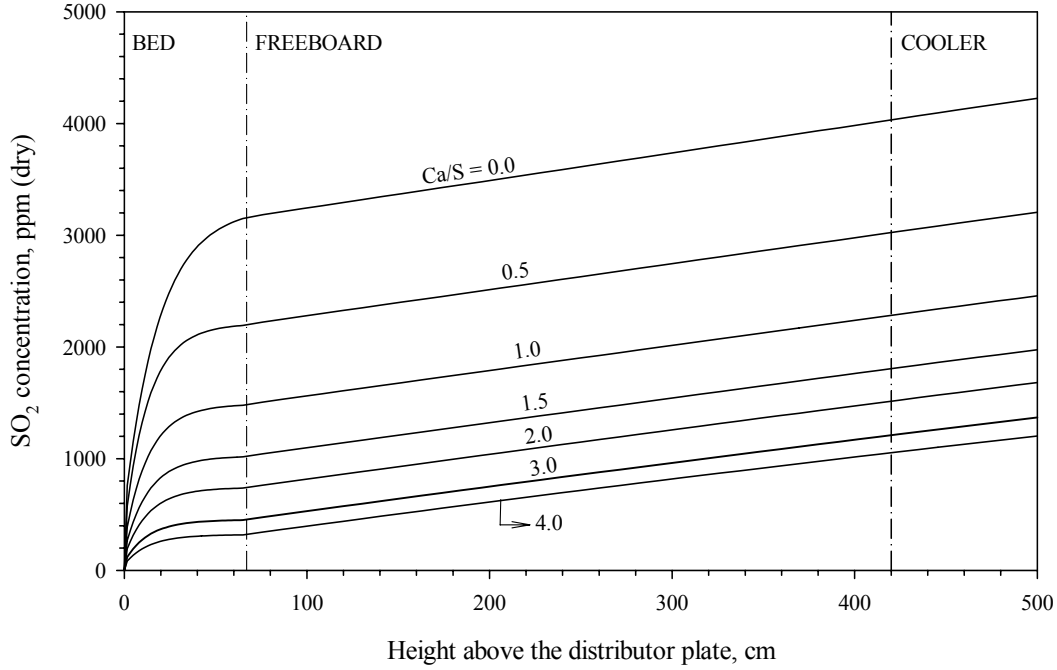

Figure 5.11 Effect of *Ca/S* on the SO_2 concentration profile (w/o recycle).

Another parametric study was performed for the effect of *Ca/S* ratio on the sulfur retention efficiency as a function of sulfation rate constant (Figure 5.12.). The figure shows that the same level of sulfur retention can be achieved by utilizing a limestone with lower sulfur capture capability but at a higher *Ca/S* ratio than the one with higher sulfur capture capability. On the other hand, there is an upper limit

of sulfur retention that can be achieved by utilizing a limestone with certain sulfur capture capability. As depicted in the figure, sulfur retention efficiency increases linearly with *Ca/S* ratio up to 1. However, with further increase in *Ca/S* ratio the slopes of the curves decrease gradually and tend to level of. Therefore, increasing the amount of sorbent in the combustor cannot always continuously increase the sulfur retention efficiency.

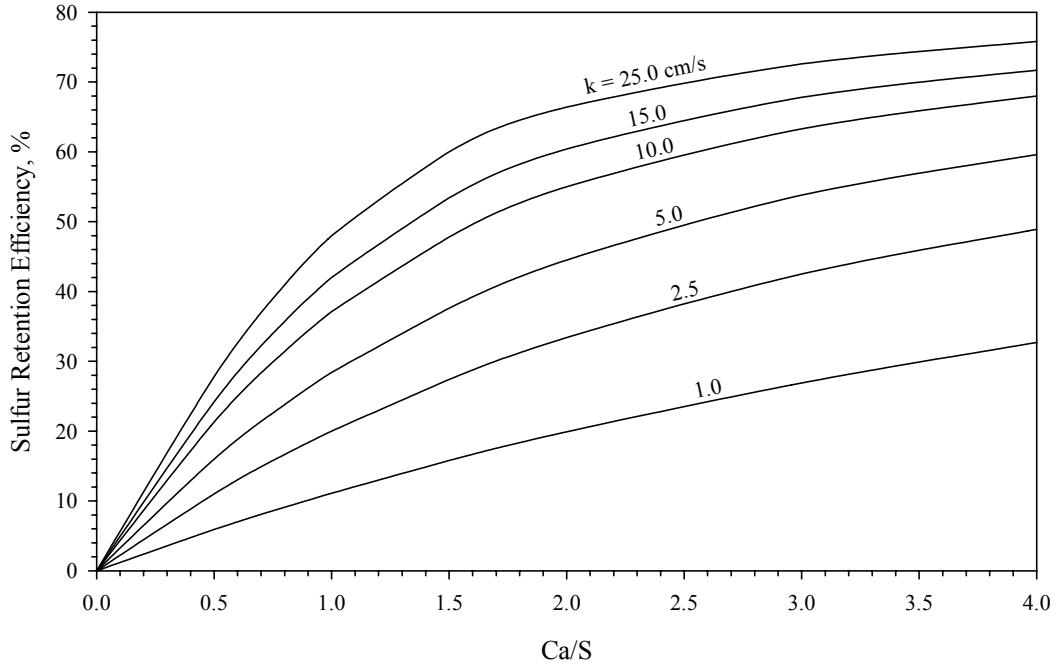

Figure 5.12 Effect of *Ca/S* ratio on the sulfur retention efficiency (w/o recycle).

Figure 5.13 illustrates the effect of recycle ratio on the sulfur retention efficiency at various *Ca/S* ratios. As can be seen from the figure, recycling enhances sulfur retention efficiency significantly up to a recycle ratio of 1.25 by increasing the residence time of elutriated sorbent particles leading to higher calcium utilization. However, as the recycle ratio is increased further, the slope of the curve decreases gradually and tends to stabilize about 1.5. It may, therefore, be concluded

that working at recycle ratios above 1.5 will not improve the sulfur capture significantly.

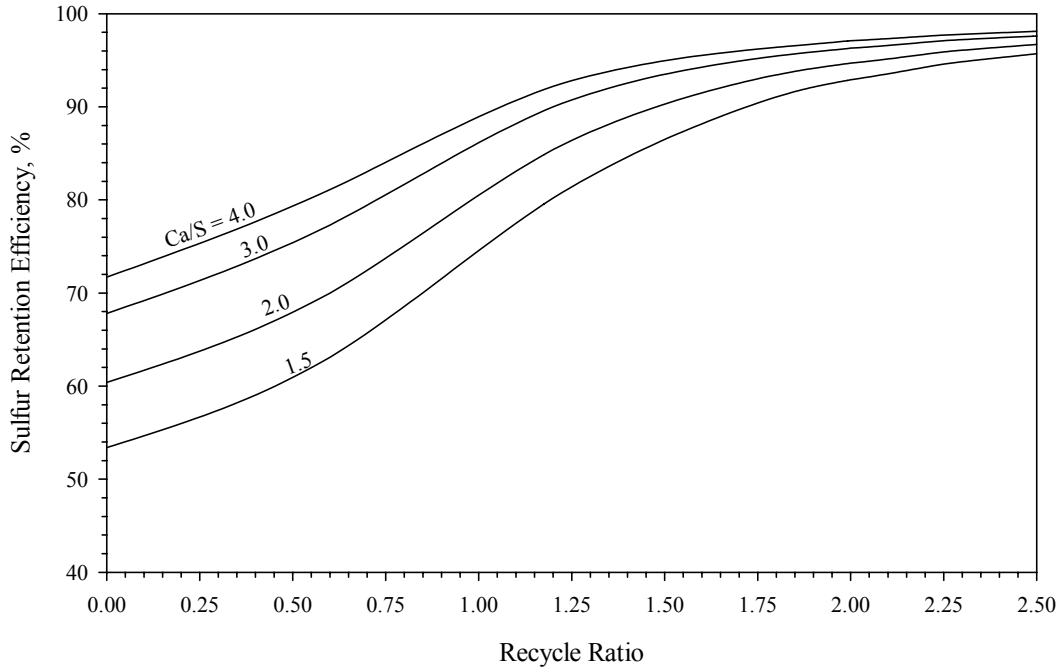

Figure 5.13 Effect of *Ca/S* ratio and recycle ratio on the sulfur retention efficiency.

CHAPTER 6

CONCLUSIONS

Sulfur retention characteristics of high sulfur containing indigenous lignites was investigated by extending a previously developed model to incorporate sulfur retention. The system model accounts for hydrodynamics, volatiles release and combustion, char combustion, particle size distribution, entrainment and elutriation and is based on conservation equations for energy and chemical species. The predictive performance of the model was tested by comparing the model predictions with measurements obtained from the combustion tests carried out by burning a typical Turkish lignite, Beypazarı, in a 0.3 MW_t Atmospheric Bubbling Fluidized Bed Combustor in its own ash at two different recycle ratios with limestone addition.

On the basis of the experimental observations and comparisons of the model predictions with measurements the following conclusions have been reached:

- O_2, O_2, CO concentration profiles and temperature profile predictions of the model are generally in good agreement with the experimental data.

- SO_2 concentration predictions throughout the combustor are in good agreement with the experimental data except for the small discrepancy between predictions and measurements in the bed section.
- Recycling enhances calcium utilization by increasing the sorbent residence time leading to higher sulfur retention efficiencies.
- Freeboard sulfur capture is enhanced significantly with recycle of elutriated sorbent particles.
- Measurements and model predictions point out that recyle is compulsory in order to obtain sulfur retention levels above 90 % in bubbling fluidized bed combustors.
- Sulfur retention efficiency is not affected significantly with further increase in recycle ratio above 1.5.

6.1 Suggestions for Future work

Based on the experience gained in the present study, the following recommendations for future extension of the work are suggested.

- Sulfation characteristics of the calcium in the fuel ash need to be investigated to obtain better sulfur capture performance while burning high inherent calcium containing lignites.
- A model for the prediction of formation and reduction of the nitrogen oxides should be incorporated into the system model in order to obtain a comprehensive model for the simulation of ABFBCs.
- A radiation model is required to be coupled to freeboard heat transfer model to predict the gas temperature in the freeboard accurately.

REFERENCES

1. Selçuk, N. and Kirmizigul, U., "Characteristics of a Fluidized-Bed Combustor Burning Low- Quality Lignite", *Journal of the Institute of Energy*, Vol. 64, 460, pp. 151-156, 1991.

2. Selçuk, N. and Tezgorucu, O., "Combustion Characteristics of Low Quality Turkish Lignites In Fluidized Bed Combustors", *Proceedings of 7th International Conference on Fluidization*, Vol. 1, pp. 505-513, New York, 1992

3. Selçuk, N., Atamer, S., Eroglu, I., Onal, I., and Kirmizigul, U., "2 MW_t Lignite Fired Atmospheric Fluidized Bed Boiler: Fundamental Process Design Philosophy", *Proceedings of the 12th International Conference on Fluidized Bed Combustion*, Vol. 1, pp. 303-308, ASME, 1993

4. Selçuk, N., "Fluidized Bed Combustion Technologies for Existing Thermal Power Plants", *Invited Paper, Workshop on Possibilities of Refurbishing Fossil-Fired Power Stations Taking into Account Environmental Requirements*, Vol. 1, pp. 241-254, Turkish Electricity Authority, Ankara, 1993

5. Oymak, O., Selcuk, N., and Onal, I., "Testing of a Mathematical-Model for the Combustion of Lignites in an AFBC", *Fuel*, Vol. 72, 2, pp. 261-266, 1993.

6. Selçuk, N., Oymak, O., and Barlas, D., "Investigation of Sulfation Characteristics of AFBC Ashes Using SEM-EDX Technique", *Proceedings of the 13th International Conference on Fluidized Bed Combustion*, Vol. 1, pp. 351-359, ASME, 1995

7. Barlas, D., Oymak, O., and Selçuk, N., "Sulfur Capture Behavior of Lignite Ash and Sorbent in AFBC's", *Preprints of International Symposium on Coal-Fired Power Generation, The Environment and Public Acceptance*, Vol. 1, pp. 259-276, Ministry of Energy and Natural Resources and Turkish Electricity Generation-Transmission Corporation, Ankara, 1995

8. Kirmizigul, U., Barlas, D., and Selçuk, N., "METU 0.3 MW AFBC Test

Rig", *Preprints of International Symposium on Coal-Fired Power Generation*, Vol. 1, pp. 257-295, Ministry of Energy and Natural Resources and Turkish Electricity Generation-Transmission Corporation, Ankara, 1995

9. Selçuk, N., Degirmenci, E., and Oymak, O., "Evaluation of an Improved Code for the Performance of AFBCs", *Journal of the Institute of Energy*, Vol. 70, 482, pp. 31-50, 1997.

10. Selçuk, N., Degirmenci, E., and Oymak, O., "Simulation of 0.3 MW_t AFBC Test Rig Burning Turkish Lignites", *Proceedings of the 14th International Conference on Fluidized Bed Combustion*, Vol. 2, pp. 1163-1174, ASME, 1997

11. Degirmenci, E. and Selçuk, N., "Dynamic Behavior of an AFBC Test Rig: An Experimental Study", *Proceedings of 15th International Conference on Fluidized Bed Combustion*, May 16-19, Savannah, GA, ASME, Paper No. FBC99-0100 (in CD-ROM), 1999

12. Organ, L. and Selçuk, N., "Transient Sulfation Behavior Limestone Particles in an AFBC Test Rig: Data for Validation Studies", *Proceedings of 15th International Conference on Fluidized Bed Combustion*, May 16-19, Savannah, GA, (Ed. R.B. Reuther), ASME, Paper No. FBC99-0101 (in CD-ROM), 1999

13. Degirmenci, E., Gogebakan, Y., and Selcuk, N., "Assessment of Catalyst Deactivation Model for Sulfur Retention in Fluidized Bed Combustors", *Combustion Science and Technology*, Vol. 153, pp. 95-111, 2000.

14. Selçuk, N. and Degirmenci, E., "Dynamic Simulation of Fluidized Bed Combustors and Its Validation Against Measurements", *Combustion Science and Technology*, Vol. 167, pp. 1-27, 2001.

15. Selçuk, N., Degirmenci, E., and Gogebakan, Y., "Modeling of a Bubbling AFBC with Volatiles Release", *Journal of Energy Resources Technology-Transactions of the Asme*, Vol. 125, 1, pp. 72-81, 2003.

16. Selçuk, N., Oymak, O., and Onal, I., "The Simulation of Atmospheric Fluidized-Bed Combustors with In-Situ Desulfurization", *Journal of the Institute of Energy*, Vol. 66, 469, pp. 159-168, 1993.

17. Selçuk, N. and Sivrioğlu, Ü. "Mathematical Modeling of Coal-Fired Fluidized Beds", *Journal of Thermal Sciences and Technology (in Turkish)*, Vol. 3, 1, pp. 31-38, 1980.

18. Selçuk, N. and Pekyılmaz, A., "Modeling of Coal-Fired Fluidized Beds", *Journal of Thermal Sciences and Technology (in Turkish)*, Vol. 5, 3, pp. 35-41, 1982.

19. Selçuk, N., Sivrioğlu, Ü., and Siddall, R. G., "Mathematical Modeling of Coal-Fired Fluidized Bed Combustors", *Proceedings of 3rd Miami Int. Conf.*

on Alternative Energy Sources, (Ed. Veziroğlu, T. N.), Vol. 6, pp. 231-256, Hemisphere Pub. Corp., New York, 1980

20. Selçuk, N., "Prediction of the Behaviour of Atmospheric Fluidized Bed Coal Combustors", *NATO ASI Series on "New Trends in Coal Science" Series C (Ed. Yürüm Y.)*, Vol. 1, pp. 495-522, Kluwer Academic Publishers, Dordrecht, Holland, 1983

21. Selçuk, N. and Pekyılmaz, A., "Modeling of Coal-Fired Fluidized Beds-Effect of Reaction Rate", *Journal of Thermal Sciences and Technology (in Turkish)*, Vol. 6, 2, pp. 39-43, 1983.

22. Selçuk, N. and Pekyılmaz, A., "Modeling of Coal-Fired Fluidized Beds-Effect of Bubble Phase Reaction", *Proceedings of the Int. Conf. "Fluidized Combustion: Is It Achiving Its Promise*, Disc 28, pp. 241-254, The Institude of Energy, London, England, 1984

23. Selcuk, N. and Özkan, Ü. "Testing of a Model for Fluidized Bed Combustors", *Proceedings of Int. Symp. on Combustion*, Vol. pp. 1471-1478, The Combustion Institude, Pittsburgh, 1985

24. Selçuk, N. and Pekyılmaz, A., "Evaluation of a Fluidized Combustor Model by Comparing Its Predictions with Measurements", *Journal of Thermal Sciences and Technology (in Turkish)*, Vol. 8, 4, pp. 31-34, 1985.

25. Selcuk, N. and Pekyılmaz, A., "Testing of a Model for Fluidized Bed Combustors-Effect of Rate Expression and Volatiles Combustion", *Proceedigs of 7th Miami Int. Conf. on Alternative Energy Sources, (Ed. Veziroğlu, T.)*, Vol. 5, pp. 337-347, Hemisphere pub. Corp., New York, 1987

26. Selcuk, N. and Pekyılmaz, A., "Testing of a Model for Fluidized Bed Combustors-Effect of Char Combustion Model", *Proceedings of Int. Symp. on Combustion*, Vol. 1, pp. 585-592, The Combustion Institude, Pittsburgh, 1987

27. Selçuk, N. and Ayyıldız, Y., "Testing of a Model for Fluidized Bed Combustors-Effect of Sherwood Number", *Proceedings of Int. Specialists' Meeting on Solid Fuel Utilization*, Vol. 4.1, pp. 1-6, The Combustion Institude (Portuguese Section), Lisbon, Portugal, 1987

28. Roostaazad, R., Selcuk, N., and Önal, I., "Literature Review on Mathematical Modeling of Atmospheric Fluidized Bed Combustors Including Freeboard Section", *Journal of Thermal Sciences and Technology (in Turkish)*, Vol. 12, 3, pp. 17-24, 1989.

29. Roostaazad, R., Selcuk, N., and Önal, I., "Mathematical Modeling of the Behavior of Atmospheric Fluidized Bed Combustors", *Proceedings of 2nd European Conf. on Industrial Furnaces and Boilers*, Vol. 2, INFUB, 1991

30. Oymak, O., Selcuk, N., and Önal, I., "Mathematical Modeling of Freeboard Section in AFBC and Testing It by Measurements", *Proceedings of 8th National Heat Transfer conference, (in Turkish)*, Vol. 1, pp. 227-239, TIBTD, 1991

31. Oymak, O., Selcuk, N., and Önal, I., "Mathematical Modeling for the Combustion of Lignites in an AFBC", *7th Int. Conf. on Fluidization*, Broadbeach, Australia, May 3-8, 1992

32. Selçuk, N., Oymak, O., and Degirmenci, E., "Basic Requirement for Modelling Fluidized Beds: Fast Computation of Particle Size Distributions (PSDs)", *Powder Technology*, Vol. 87, 3, pp. 269-271, 1996.

33. Selcuk, N., Degirmenci, E., and Oymak, O., "Simulation of 0.3 MW_t AFBC Test Rig Burning Turkish Lignites", *Proceedings of the 14th Int. Conf. on Fluidized Bed Combustion, (Ed. Preto, F. D. S.)*, Vol. 2, pp. 1163-1174, 1997

34. Bethell, F. V., Gill, D. W., and Morgan, B. B., "Mathematical Modeling of the Limestone-Sulfur Dioxide Reaction in a Fluidized-Bed Combustor", *Fuel*, Vol. 52, pp. 121-127, 1973.

35. Chen, T. P. and Saxena, S. C., "Mathematical Modeling of Coal Combustion in Fluidized Beds with Sulfur Emission Control by Limestone or Dolomite", *Fuel*, Vol. 56, pp. 401-413, 1977.

36. Rajan, R., Krishnan, R., and Wen, C. Y., "Simulation of Fluidized Bed Combustors Part II. Coal Devolatilization and Sulfur Oxides Retention", *The American Institude of Chemical Engineers Symposium Series*, Vol. 74, No:176, 1978

37. Rajan, R. and Wen, C. Y., "A Comprehensive Model for Fluidized Bed Combustors", *AIChE Journal*, Vol. 26, 4, pp. 642-655, 1980.

38. Lee, D. C., Hodges, L., and Georgakis, C., "Modeling of SO_2 Emissions from Fluidized Bed Coal Combustors", *Chemical Engineering Science*, Vol. 35, pp. 302-306, 1980.

39. Lee, D. C. and Georgakis, C., "A Single, Particle-Size Model for Sulfur Retention in Fluidized-Bed Coal Combustors", *AIChE Journal*, Vol. 27, 3, pp. 472-481, 1981.

40. Zheng, J., Yates, J. G., and Rowe, P. N., "A Model for Desulphurisation with Limestone in A Fluidised Coal Combustor", *Chemical Engineering Science*, Vol. 37, 2, pp. 167-174, 1982.

41. Fee, D. C., Wilson, W. I., Myles, K. M., and Johnson, I., "Fluidized-Bed Coal Combustion: In-Bed Sorbent Sulfation Model", *Chemical Engineering Science*, Vol. 38, 11, pp. 1917-1925, 1983.

42. Fee, D. C., Myles, K. M., Marroquin, G., and fan, L.-S., "An Analytical Model for Freeboard and In-Bed Limestone Sulfation in Fluidized-Bed Coal Combustors", *Chemical Engineering Science*, Vol. 39, 4, pp. 731-737, 1984.

43. Ho, T. C., Lee, H. T., and Hopper, J. R., "Simulation of Desulfurization in a Fluidized-Bed Limestone Reactor", *AIChE Journal*, Vol. 32, 10, pp. 1754-1759, 1986.

44. Hodges, J. L., Jukkola, G. D., and Kantesaria, P. P., "Model Predictions of Combustion and Sulfur Capture Processes in AFBC", *Proceedings of the 9th Int. Conf. on Fluidized Bed Combustion*, Vol. 1, pp. 494-500, The American Society of Mechanical Engineers, Boston USA, 1987

45. Schouten, J. C. and van den Bleek, C. M., "The D.U.T. SURE Model: A Simple Approach in FBC Sulfur Retention Modeling", *Proceedings of 9th International Conference on Fluidization*, Vol. 1, pp. 749-761, Boston, 1987

46. Schouten, J. C. and van den Bleek, C. M., "The Influence of Oxygen-Stoichiometry on Desulfurization During FBC: A Simple Sure Modeling Approach", *Chemical Engineering Science*, Vol. 43, 8, pp. 2051-2059, 1988.

47. Dennis, M. A. and Hayhurst, A. N., "A Model for the Continuous Desulphurisation of a Fluidised Bed Combustor Using Limestones, Dolomites or Related Solid Sorbents", *Journal of the Institude of Energy*, pp. 98-109, 1988.

48. Dennis, M. A. and Hayhurst, A. N., "A Simplified Analytical Model for the Rate of Reaction of SO_2 with Limestone Particles", *Chemical Engineering Science*, Vol. 41, 1, pp. 25-36, 1986.

49. Zhang, J. Q. and Anthony, E. J., "Development of Analytical One-Phase Models for Sulphur Retention in Fluidized Bed Combustors", *Proceedings of the Int. Conf. on Fluidization VI, (Ed. Grace, J. R., Shemilt, L. W.,Bergougnou, M. A.)*, Vol. 1, pp. 411-419, May 7-12, Canada, 1989

50. Lin, W., Senary, M. K., and Van den Bleek, C. M., "SO_2/NO_x Emissions in FBC of Coal: Experimental Validation of The DUT SURE-Model with Data from the Babcock and Wilcox 1-Foot x 1-Foot AFBC Unit", *Proceedings of the 11th Int. Conf. on Fluidized Bed Combustion*, Vol. 1, pp. 649-654, ASME, Montreal, Canada, 1991

51. Lin, W., Valkenburg, P. J. M., and Van den Bleek, C. M., "Prediction of NO_x and SO_x Emissions in FBC of Coal Using Easy to Determine Coal and Sorbent Characteristics", *Fuel Processing Technology*, Vol. 24, pp. 399-405, 1990.

52. Rubiera, F., Labiano, G. F., Fuertes, A. B., Pis, J. J., and Adanez, J., "Characterization of the Reactivity of Limestone with SO_2 in a Fluidized Bed Reactor", *Proceedings of the 2nd European Conf. on Industrial Furnaces and Boilers*, Vol. 1, April 2-5, Portugal, 1991

53. Lin, W., Svoboda, K., and Van den Bleek, C. M., "Sulphur Capture and Its Interactions with NO_x Emissions in Fluidized Bed Combustion of Coal: General Analytical Model Based on Particle Gas-Solid Reactions", *Chemical Engineering Science*, Vol. 47, 9-11, pp. 2425-2430, 1992.

54. Lin, W., Bu, J., Korbee, R., and Svoboda, K., "Modelling SO_2 and NO_x Emissions in Fluidized Bed Combustion of Coal", *Fuel*, Vol. 72, pp. 299-304, 1993.

55. Walsh, P. M., "A Descriptive Model for Sulfur Capture in Bubbling Atmospheric Pressure Fluidized Bed Combustors", *Proceedings of the 13th Int. Conf. on Fluidized Bed Combustion*, Vol. 1, pp. 341-350, ASME, 1995

56. Huilin, L., Guangbu, Z., Ruoshan, B., Lidan, Y., and Yukun, Q., "Modeling of Coal Combustion in a 25-MW FBC Power Plant", *Energy*, Vol. 24, pp. 199-208, 1999.

57. Lyngfelt, A. and Leckner, B., "Sulphur Capture in Circulating Fluidized-Bed Boilers: Can the Efficiency Be Predicted?" *Chemical Engineering Science*, Vol. 54, 22, pp. 5573-5584, 1999.

58. Selçuk, N., Göğebakan, Y., Harmandar, H., and Altındağ, H., "Effect of Recycle on Fluidized Bed Combustion and Emission Characteristics of High Sulfur Lignite", *Proceedinds of the 3rd Mediterranean Combustion Symp.*, Vol. 1, pp. 227-236, Marrakech, Morocco, June 8-13, 2003

59. Degirmenci, E. and Selcuk, N., "Dynamic Behavior of an AFBC Test Rig: An Experimental Study (Ed. Reuther, R. A.)", *15th Int. Conf. on Fluidized Bed Combustion*, Paper No:100 (in CD-ROM), ASME, Savannah, USA, 1998

60. Degirmenci, E., "*Dynamic Simulation of Fluidized Bed Combustors*", Ph.D, Department of Chemical Engineering, METU, Turkey, 2000

61. Jung, K. and La Nauze, R. D., "Sherwood Numbers for Burning Particles in Fluidized Beds", *Proceedings of the 4th Int. Conf. on Fluidization*, Vol. 1, pp. 427-434, Engineering Foundation, Koshikojima, Japan, 1983

62. Incropera, F. P. and De Witt, D. P., Fundementals of Heat and Mass Transfer, 3rd ed, *John Wiley and Sons*, New York,1990.

63. Choi, J. C., Chang, I. Y., Shun, D. W., Yi, C. K., Son, J. E., and Kim, S. D., "Correlation on the Particle Entrainment Rate in Gas Fluidized Beds", *Ind. Eng. Chem. Res.*, Vol. 38, pp. 2491-2496, 1999.

64. Kunii, D. and Levenspiel, O., Fluidization Engineering, 2nd Ed., *Butterworth Heinemann*, Boston, 1991.

65. Davidson, J. F., Clift, R., and Harrison, D., Fluidization, 2nd Ed., *Academic Press*, London, 1985.

66. Ergun, S., "Fluid Flow Through Packed Columns", *Chemical Engineering Progress*, Vol. 48, pp. 89-94, 1952.

67. Mori, S. and Wen, C. Y., "Estimation of Bubble Diameter in Gaseous Fluidized Bed", *AIChE Journal*, Vol. 21, 1, pp. 109-116, 1975.

68. Gogolek, P. E. G. and Besker, H. A., "Calculation of the Expansion of a Bubbling Fluidised Bed of Coarse Particles", *Powder Technology*, Vol. 71, pp. 107-110, 1992.

69. Denloye, A. O. O. and Botterill, J. S. M., "Bed to Surface Heat Transfer in a Fluidized Bed of Large Particles", *Powder Technology*, Vol. 19, pp. 197-203, 1978.

70. Sleicher, C. A. and Rouse, M. W., "A Convenient Correlation for Heat Transfer to Constant and Variable Property Fluids in Turbulent Pipe Flow", *Int. Journal of the Heat and Mass Transfer*, Vol. 18, pp. 677-683, 1975.

71. Field, M. A., Gill, D. W., Morgan, B. B., and Hawksley, P. G. W., "Combustion of Pulverized Coal", *British Coal Utilization Research Association, Leatherland*, pp. 186-209, 322-325, 1967

72. Hottel, H. C., Williams, G. C., Nerheim, N. M., and Schneider, G. R., "Kinetic Studies on Stirred Reactors, Combustion of Carbon Monoxide and Propane", *Proceedings of the 10th Int. Symp. on Combustion*, Vol. 1, pp. 975-986, The Combustion Institude, Pittsburgh, 1965

73. Grace, J. R. and Clift, R., "On the Two Phase Theory of Fluidization", *Chemical Engineering Science*, Vol. 24, pp. 327-334, 1974.

74. Grace, J. R. and Harrison, D., "The Behaviour of Freely Bubbling Fluidized Beds", *Chemical Engineering Science*, Vol. 24, pp. 497-508, 1969.

75. Davidson, J. F. and Harrison, D., Fluidised Particles, *Cambridge University Press*, London, 1963.

76. Hannes, J., "*Mathematical Modelling of Circulating Fluidized Bed Combustion*", Ph. D., RTWH Aachen, Germany, 1996

77. Stubingon, J. F., Chan, S. W., and Clough, S. J., "A Model for Volatiles Release into a Bubbling Fluidized-Bed Combustor", *AIChE Journal*, Vol. 36, 1, pp. 75-85, 1990.

78. Anthony, D. B. and Howard, J. B., "Coal Devolatilization and Hydrogasification", *AIChE Journal*, Vol. 22, 4, pp. 625-656, 1976.

79. Göğebakan, Y., "*Char Attrition in Fluidized Bed Combustors*", M. Sc., Department of Chemical Engineering, METU, Turkey, 2000

80. Illerup, J. B., Dam-Johansen, K., and Lunden, K., "Hıgh-Temperature Reaction Between Sulfur Dioxide and Limestone-VI. The Influence of High

Pressure", *Chemical Engineering Science*, Vol. 48, 11, pp. 2151-2157, 1993.

81. Scala, F., Cammarota, A., Chirone, R., and Salatino, P., "Comminution of Limestone During Batch Fluidized-Bed Calcination and Sulfation", *AIChE Journal*, Vol. 43, 2, pp. 363-373, 1997.

82. Marsh, D. W. and Ulrichson, D. L., "Rate and Diffusional Study of the Reaction of Calcium Oxide with Sulfur Dioxide", *Chemical Engineering Science*, Vol. 40, 3, pp. 423-433, 1985.

83. Adanez, J., Labiano, G. F., and Gayan, P., "Sulfur Retention in AFBC. Modeling and Sorbent Characterization Methods", *Fuel Processing Technology*, Vol. 36, pp. 73-79, 1993.

84. Vleeskens, J. M., van Haasteren, T. W. M. B., and Roos, M., "Behaviour of Different Char Components in Fluidized Bed Combustion: A Char Petrography Study", *Fuel*, Vol. 67, pp. 426-430, 1988.

85. Hazlett, J. D. and Bergougnou, M. A., "Influence of Bubble Size Distribution at the Bed Surface on Entrainment Profile", *Powder Technology*, Vol. 70, pp. 99-107, 1992.

86. Kunii, D. and Levenspiel, O., "Fluidized Reactor Models. 1. For Bubbling Beds of Fine, Intermediate, and Large Particles. 2. For the Lean Phase: Freeboard and Fast Fluidization", *Ind. Eng. Chem. Res.*, Vol. 29, pp. 1226-1234, 1990.

87. Radhakrishnan, K. and Hindmarsh, A. C., "Description and use of LSODE, the Livermore Solver for Ordinary Differential Equations", *Lawrance Livermore National Laboratory Report No: UCRL-ID-113855*, 1993

88. Anthony, E. J., Couturier, M. F., and Briggs, D. W., "Gas Sampling at the Point Tupper AFBC Facility", *Division Report 86-70 (TR), CANMET*, Energy, Mines and Resources, Canada, 1986

89. Harmandar, H., "*Effect of Recycling on the Performance of Bubbling Fluidized Bed Combustors*", M. Sc., Department of Chemical Engineering, METU, Turkey, 2003

90. Chakraborty, R. K. and Howard, J. R., "Combustion of Char in Shallow Fluidized-Bed Combustors - Influence of Some Design and Operating Parameters", *Journal of the Institute of Energy*, Vol. 54, 418, pp. 48-54, 1981.

91. Tartan, M., "*In-Situ Desulfurization in an Atmospheric Fluidized Bed Combustor*", M. Sc., Department of Chemical Engineering, METU, Turkey, 1991

APPENDIX A

GAS INTERCHANGE COEFFICIENT

The expression utilized in the original system model for the prediction of the combustion behavior was [86]:

$$K_{be} = 4.5\frac{u_e}{d_b} \tag{A.1}$$

Gas interchange coefficients calculated by using Equation (A.1) and Equation (3.5) for all Runs are presented in Table A.1. As can be seen from the table, gas interchange coefficients calculated by using Equation (A.1) are much lower than those determined from Equation (3.5), leading to insufficient gas exchange between bubble and emulsion phases. This may be considered to be due to the fact that the expressions for the determination of gas interchange coefficient are adapted to cold systems. However, at elevated temperatures values higher than 40 s^{-1} were reported in the literature [76]. For this reason, the values obtained from Equation (3.5), which are higher than 40 s^{-1}, are more consistent. Therefore, in this thesis study it is preferred to use Equation (3.5) instead of Equation (A.1), which was used in the

original system model [60] for the prediction of the combustion behavior.

Table A.1 Comparison of gas interchange coefficients.

	K_{be} (from Equation (3.5)), s^{-1}	K_{be} (from Equation (A.1)), s^{-1}
Run 1	46.3	29.2
Run 2	52.4	33.1
Run 3	48.8	30.5

APPENDIX B

SULFATION RATE CONSTANT

Overall sulfation rate constant, k, is a combination of mass transfer limitations and sulfation kinetics,

$$\frac{1}{k} = \frac{1}{k_s} + \frac{1}{k_f} \tag{B.1}$$

where k_f and k_s are mass transfer coefficient and kinetic rate constant, respectively. Mass transfer coefficient can be calculated by using,

$$k_f = \frac{D_{SO_2} Sh}{d_{lst}} \tag{B.2}$$

where Sh and D_{SO_2} are Sherwood number and diffusivity of SO_2 in air, respectively. Sherwood number can be calculated by the expression suggested by Chakraborty and Howard [90]:

$$Sh = 2\varepsilon + 0.69\, Re^{1/2}\, Sc^{1/3} \qquad \text{(B.2)}$$

In order to observe the dependency of overall sulfation rate constant on the sorbent particle size, kinetic rate constant is fixed at 15 *cm/s*, which is in the middle of the range (5-30 *cm/s*) given in the literature [45]. Overall sulfation rate constant, which is calculated by using Equation (B.1) and mass transfer coefficient are presented in Figure B.1 as a function of sorbent particle size. As depicted in the figure, although mass transfer coefficient strongly depends on the sorbent particle size, overall sulfation rate constant is almost independent of it.

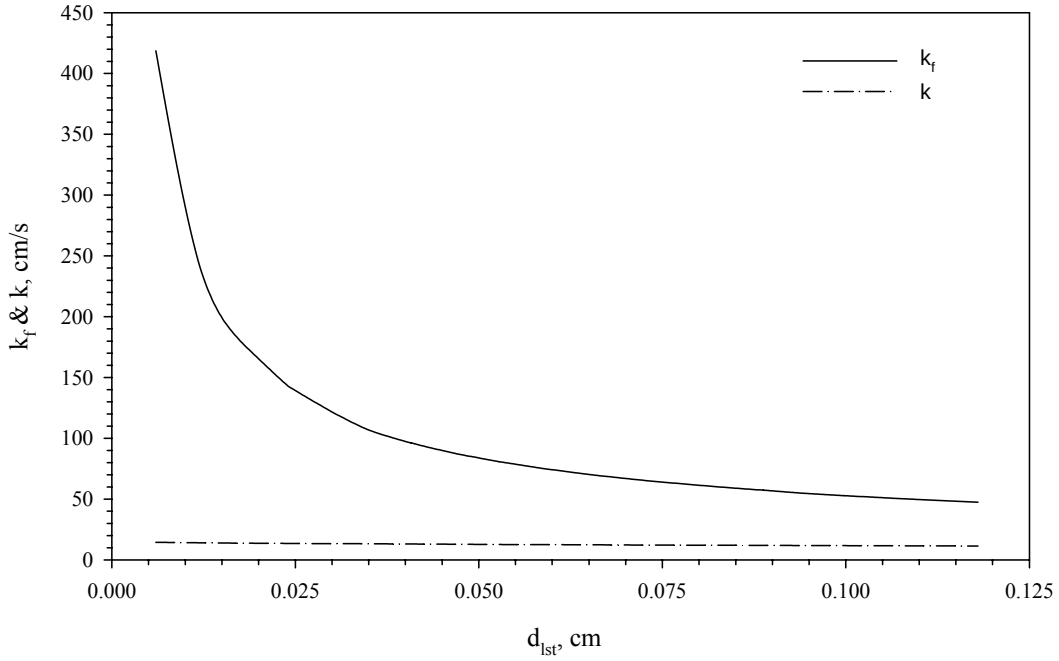

Figure B.1 Mass transfer coefficient, k_f, and overall sulfation rate constant, k, as a function of sorbent particle size.

APPENDIX C

ESTIMATION OF NUMBER OF CYCLES OF RECYCLED PARTICLES

The number of cycles of the recycled ash and sorbent particles through the combustion zone, N_r, can be determined by Equation (3.37). It may be more convenient to explain this approximation in an example situation. A simple diagram of an ABFBC at steady state operation with recycling of elutriated particles is presented in Figure C.1. As can be seen from the figure, 50 % of the cyclone ash is recycled back to combustor while the other half is discharged. The amount of elutriated and recycled sorbent and ash particles is 20 *kg/h*. Therefore, in every hour of operation 20 *kg/h* elutriated particles are captured by the cyclone. If 10 *kg/h* of recycled particles are considered, they have to complete one cycle and have to be discharged in the next in order to prevent accumulation in the system. Otherwise, if they complete more than one cycle, the freshly elutriated particles will have to be discharged without recycling back to the combustor. Therefore, the number of cycles should be 1, which is the same number as estimated by Equation (3.37) for

the example situation under consideration. The number of cycles in the experiments carried out in this study (Run 2 and 3) is estimated to be about 3.

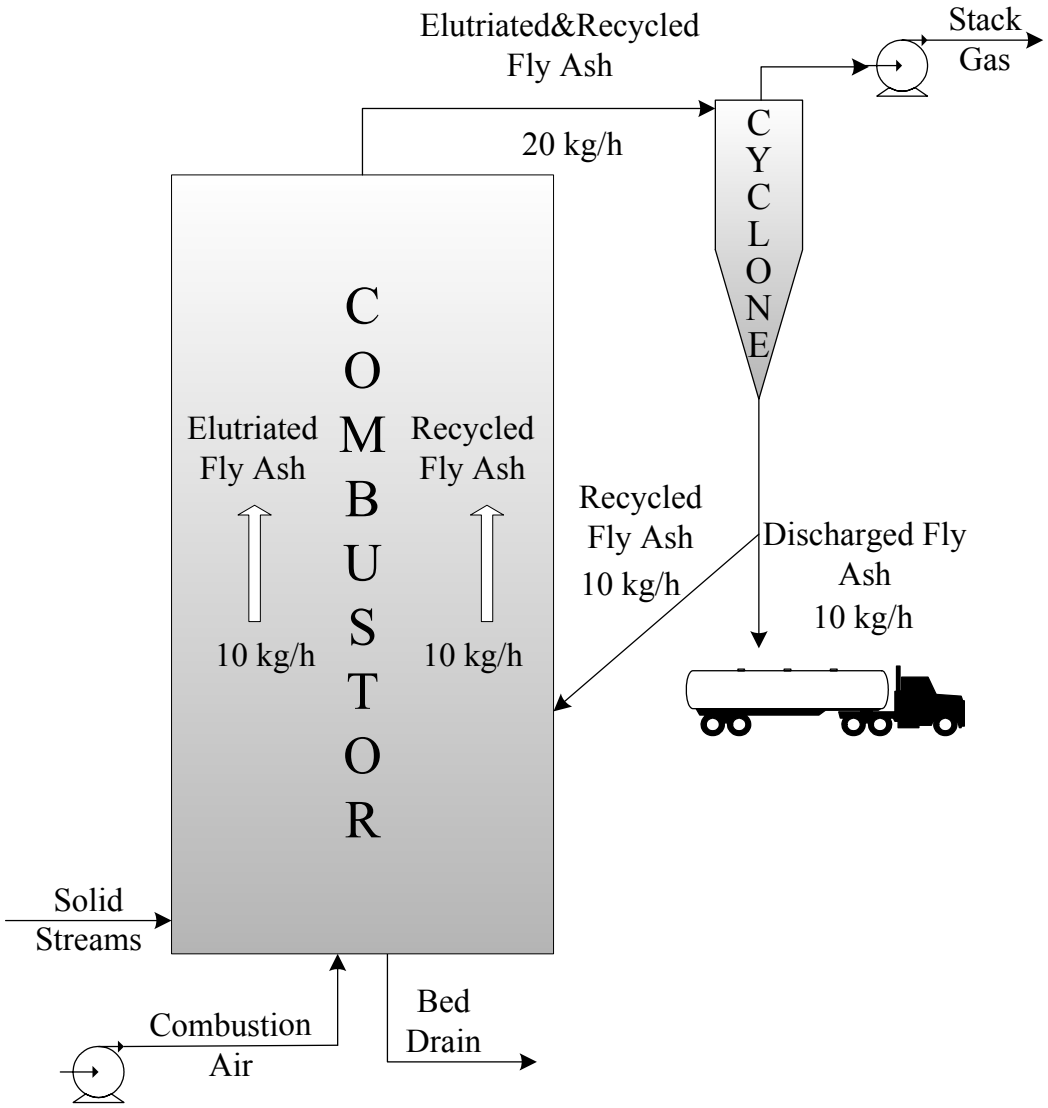

Figure C.1 A simple diagram of an ABFBC at steady operation with recycle.

APPENDIX D

ROSIN-RAMMLER SIZE DISTRIBUTION FUNCTIONS

The coal and limestone particle size distributions were determined by sieve analysis, which was expressed by Rosin-Rammler size distribution function in the system model:

$$P_o\left(d_p\right) = exp\left[-bd_p^n\right] \tag{D.1}$$

In order to obtain coefficients of Rosin-Rammler function Curve Expert 1.3 was used. Table D.1 shows the Rosin-Rammler size distribution function coefficients, standard errors and correlation coefficients obtained by fitting size distributions of both lignite and limestone to Rosin Rammler function.

Table D.1 Rosin-Rammler function fitting results of lignite and limestone.

	Lignite	**Limestone**
b	14.14	86.31
n	1.79	1.60
Standard Error	0.04	0.05
Correlation Coefficient	0.99	0.99

Fitted Rosin-Rammler forms of lignite and limestone are presented in Figures D.1 and D.2. As can be seen from the figures, Rosin- Rammler function represents size distributions of limestone and lignite reasonably accurately.

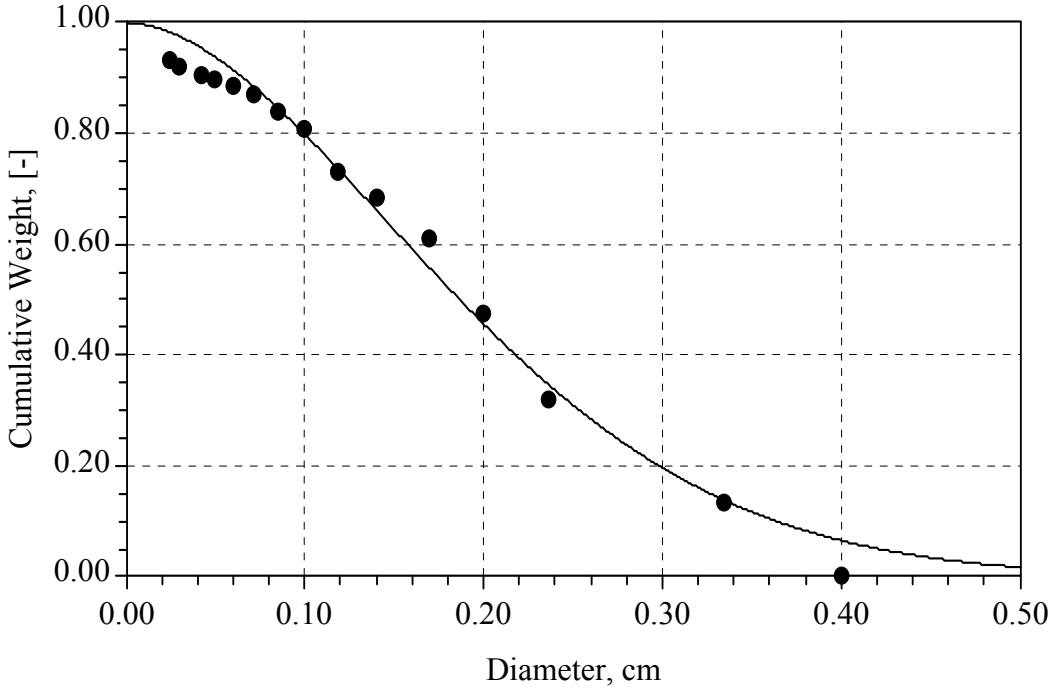

Figure D.1 Fitted Rossin-Rammler form of Beypazarı lignite.

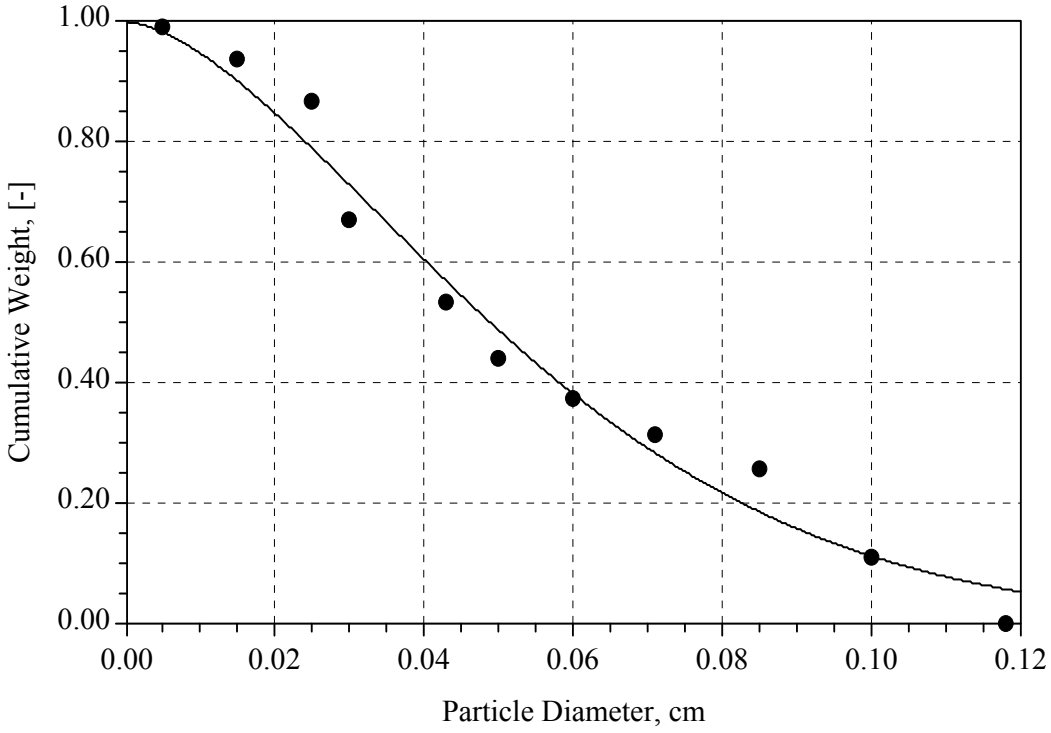

Figure D.2 Fitted Rossin-Rammler form of Beypazarı limestone.

APPENDIX E

CHEMICAL ANALYSES OF ASH STREAMS

Table E.1 Chemical analyses of final bed material and bed drains for all runs.

	BED DRAIN			BED
	Run 1	**Run 2**	**Run 3**	**ASH**
SiO_2, %	29.82	9.56	24.94	27.90
Al_2O_3, %	11.78	3.69	3.66	10.29
Fe_2O_3, %	6.27	3.54	4.68	4.88
CaO, %	33.10	56.35	44.80	26.90
MgO, %	1.99	1.49	2.74	2.65
SO_3, %	12.80	27.03	18.53	15.68
Na_2O, %	2.49	1.20	2.09	2.63
K_2O, %	1.51	0.60	1.02	1.51
TiO_2, %	0.74	0.46	0.67	0.70

Table E.2 Chemical analyses of cyclone ashes for all runs.

	Run 1	**Run 2**	**Run 3**
SiO_2, %	26.82	30.10	32.90
Al_2O_3, %	10.43	9.30	10.75
Fe_2O_3, %	7.81	6.00	6.86
CaO, %	24.10	24.48	34.05
MgO, %	1.74	1.45	1.87
SO_3, %	11.32	14.87	11.87
Na_2O, %	4.31	3.37	3.77
K_2O, %	0.90	0.84	0.96
TiO_2, %	1.47	1.12	1.38

Table E.3 Chemical analyses of baghouse filter ashes for all runs.

	Run 1	**Run 2**	**Run 3**
SiO_2, %	17.92	17.54	17.04
Al_2O_3, %	7.17	6.98	7.53
Fe_2O_3, %	11.29	11.42	11.21
CaO, %	21.85	27.78	29.68
MgO, %	3.52	3.11	3.77
SO_3, %	19.47	16.67	19.82
Na_2O, %	4.58	2.02	1.62
K_2O, %	1.08	1.08	1.14
TiO_2, %	3.87	3.90	4.28

APPENDIX F

SULFUR CAPTURE CAPABILITY OF BEYPAZARI LIMESTONE

Table F.1 Required data and calculated sulfur capture capability of Beypazarı limestone for all runs (based on combustible sulfur content).

	Run 1	**Run 2**	**Run 3**
Coal flow rate (wet*), kg/h*	101.7	101.7	101.7
Limestone flow rate (wet), *kg/h*	24.69	25.56	33.42
Sulfur (combustible, wet), *%*	2.49	2.49	2.49
CaCO3, (dry) *%*	94.73	94.73	94.73
Limestone Moisture, %	0.93	0.93	0.93
Stack gas flow rate (dry), *kmol/h*	18.2	17.2	18.0
SO2 emission (dry), *ppm*	1369	872	282
Ca/S (based on combustible sulfur content)	3.0	3.1	4.0
Sulfur in, *kmol/h*	0.079	0.079	0.079
Sulfur out, *kmol/h*	0.025	0.015	0.005
CaCO3 in, *kmol/h*	0.232	0.240	0.314
Reactivity, *g Sulfur / kg CaCO3*	**74.9**	**86.4**	**76.3**

Table F.2 Required data and calculated sulfur capture capability of Beypazarı limestone for all runs (based on total sulfur content).

	Run 1	**Run 2**	**Run 3**
Coal flow rate (wet), *kg/h*	101.7	101.7	101.7
Limestone flow rate (wet), *kg/h*	24.69	25.56	33.42
Sulfur (total, wet), *%*	4.1	4.1	4.1
$CaCO_3$, (dry) *%*	94.73	94.73	94.73
Limestone Moisture, *%*	0.93	0.93	0.93
Stack gas flow rate (dry), *kmol/h*	18.2	17.2	18.0
SO_2 emission (dry), *ppm*	1369	872	282
Ca/S (based on total sulfur content)	1.8	1.8	2.4
Sulfur in, *kmol/h*	0.130	0.130	0.130
Sulfur out, *kmol/h*	0.025	0.015	0.005
$CaCO_3$ in, *kmol/h*	0.232	0.240	0.314
Reactivity, *g Sulfur / kg CaCO3*	**145.5**	**153.8**	**127.8**

Sulfur capture capability of Beypazarı limestone is calculated for all runs by using the following calculation procedure:

$$Sulfur\ in\ \left(kmol/h\right) = \frac{coal\ feed\left(kg/h\right) \times fraction\ of\ sulfur\ in\ coal}{MW\ of\ sulfur\left(kg/kmol\right)} \qquad \text{(F.1)}$$

Sulfur leaving the combustor can be determined by the following two alternatives depending on the available data:

If stack gas flow rate and emission of SO_2 is known,

$$Sulfur\ out\ \left(kmol/h\right) = Stack\ gas\ flow\ rate\left(kmol/h\right) \times fraction\ of\ SO_2 \qquad \text{(F.2)}$$

alternatively, if sulfur retention is known:

$$Sulfur\ out\ \left(kmol/h\right) = \left(1 - \frac{Sulfur\ retention\ efficiency}{100}\right) \times sulfur\ in\ \left(kmol/h\right) \qquad \text{(F.3)}$$

Captured sulfur can then be easily calculated by taking the difference:

$$Captured\ sulfur\ \left(kmol/h\right) = \left(sulfur\ in - sulfur\ out\right)\left(kmol/h\right) \qquad \text{(F.4)}$$

The amount of input $CaCO_3$ is calculated from the limestone flow rate:

$$CaCO_3 \text{ in (kg/h)} = \text{limestone flow rate}\left(kg/h\right) \times \text{fraction of } CaCO_3 \quad \text{(F.5)}$$

Finally, the sulfur capture capability of limestone under fluidized bed combustion conditions can be found by:

$$\text{Reactivity}\ \left(g\ S / kg\ CaCO_3\right) = \frac{\text{Sulfur captured}\left(g/h\right)}{CaCO_3 \text{ in } \left(kg/h\right)} \quad \text{(F.6)}$$

APPENDIX G

POINT VALUES OF MEASUREMENTS

Table G.1 Thermocouple readings for all runs.

Thermocouple		**Temperature,** *°C*		
No	**Height,** *cm*	**Run 1**	**Run 2**	**Run 3**
1	25	856	832	823
2	44	854	830	821
3	73	848	824	816
4	73	853	830	820
5	97	855	832	822
6	133	865	858	840
7	154	865	860	843
8	226	862	873	847
9	257	865	883	852
10	285	857	879	846
11	330	838	864	831
12	361	825	855	820
13	425	737	759	713
14	500	372	364	338

Table G.2 Sampling probe readings of O_2, CO_2 and CO concentrations for all runs, *dry mole %.*

Probe		**Run 1**			**Run 2**			**Run 3**		
No	**Height,** c*m*	***O_2***	***CO_2***	***CO***	***O_2***	***CO_2***	***CO***	***O_2***	***CO_2***	***CO***
1	500	6.66	12.95	0.1943	5.97	13.42	0.2058	5.37	14.02	0.1735
2	419	6.30	13.39	0.1986	6.06	12.97	0.2150	-	-	-
3	344	6.84	12.90	0.1847	6.00	13.39	0.1960	-	-	-
4	291	7.03	12.38	0.1944	-	-	-	-	-	-
5	183	8.05	11.70	0.2091	7.43	11.46	0.2657	-	-	-
6	123	9.13	10.59	0.2583	-	-	-	-	-	-
7	85	-	-	-	-	-	-	-	-	-
8	69	6.88	11.86	1.0552	-	-	-	-	-	-
9	56	7.48	11.12	0.9695	6.61	12.14	0.9574	-	-	-
10	26	8.16	10.69	0.8012	-	-	-	-	-	-

Table G.3 Sampling probe readings of SO_2 concentrations for all runs.

Probe		***SO_2*, *(dry), ppm***		
No	**Height,** *m*	**Run 1**	**Run 2**	**Run 3**
1	500	3678	4314	4079
2	419	3703	-	-
3	344	3178	-	3892
4	291	3315	-	-
5	183	2726	-	-
6	123	-	3105	3052
7	85	1551	-	-
8	69	1167	-	-
9	56	853	-	1055
10	26	429	-	-